THE UNIVERSITY OF QUEENSLAND
AUSTRALIA

THZ evaluation of hydration of different creams on human skin

by

Diewen Yang

School of Electrical Engineering and Computer Science

The University of Queensland.

Submitted for the degree of Master of Computer Science in the division of Computer Science.

3rd June 2024

Diewen Yang

s4595136@uqconnect.edu.au

3rd June 2024

Prof Michael Brünig,
Head of School
School of Electrical Engineering and Computer Science
The University of Queensland
St Lucia QLD 4072

Dear Professor Brünig,

In accordance with the requirements of the Degree of Master of Computer Science in the School of Electrical Engineering and Computer Science, I submit the following thesis entitled

"THZ evaluation of hydration of different creams on human skin"

The thesis was performed under the supervision of Dr. Xiaoqiong Qi. I declare that the work submitted in the thesis is my own, except as acknowledged in the text and footnotes, and that it has not previously been submitted for a degree at the University of Queensland or any other institution.

Yours sincerely

Diewen Yang

Acknowledges

I am very grateful to my supervisor, Tina Qi, for her thorough and detailed guidance in the completion of my research, from choosing the topic of the thesis, developing the proposal, and completing the experiments, all of which took a great deal of her time.

Thank you to my family and friends who love me all the time.

Finally, thanks to myself, she persisted in her choice to study computer science, which was difficult but rewarding for her.

Abstract

The use of terahertz imaging to assess the efficacy of different types of creams in moisturizing the skin has become a potentially valuable area of research. The key to testing the effectiveness of moisturization is the degree of signal feedback from the terahertz imaging technique on the water content of the skin surface. Previous studies have shown that TDS systems used for terahertz imaging to assess hydration in the human body not only have poor resolution and small available signal-to-noise ratios (SNR) but also acquire spectral data slowly. Therefore, we performed terahertz imaging based on laser feedback interferometry in a terahertz quantum cascade laser and used traditional electrical methods as a reference experiment. Changes in the water content of the skin surface over time were shown by the signal strength of the feedback, thus observing differences in the efficacy of the creams. The experimental results and data analyses show that the Thz-QCL technique is effective in determining the moisturizing effect of different creams. Thus, the LFI technique opens new avenues in the field of evaluating the efficacy of skin care products.

Contents

Chapter 1. List of Figures

Chapter 2. Introduction:

The key factor determining whether skin barrier protection functions properly is the state of the skin surface, especially its water content [1]. The moisture content of the skin directly affects its barrier function. Adequate hydration can help maintain the skin's softness and smoothness, as well as improve its ability to resist external environmental factors such as pollutants and allergens [2]. Conversely, inadequate skin hydration can lead to dry, rough skin that is more susceptible to forming fine lines and wrinkles. In addition, this may damage the integrity of the skin barrier, leading to a range of dermatological conditions [3]. Creams possess significant moisturizing properties and are an essential component of a basic skincare routine. Therefore, the evaluation of their moisturizing effects has attracted the attention of researchers.

In recent years, there has been a growing trend to use terahertz imaging to assess the water content of the skin surface. The first reason is that it is a non-invasive real-time imaging technique capable of acquiring data without destroying the skin surface [4]. In addition, the high sensitivity of terahertz to moisture provides a great facility for determining skin water content. When subtle changes occur in the skin, terahertz transmits information about the changes to the observer through the radiation response, thus enabling highly accurate water content detection [5].

Over the past decades, most terahertz imaging for assessing human hydration has used time-domain spectroscopy (TDS) techniques. TDS has become the primary method for identifying objects with different morphologies at terahertz frequencies [6]. However, TDS systems not only have poor resolution and limited signal-to-noise ratio (SNR) availability but also slow spectral data acquisition [7]. These limitations make TDS inadequate for evaluating the instantaneous effects of creams on the skin.

To address these issues, we implemented terahertz imaging based on laser feedback interferometry in a terahertz quantum cascade laser (QCL). This approach provides significantly higher spectral resolution and considerably greater output power compared to traditional TDS systems [8]. These properties allow the QCL to provide clearer and more detailed skin imaging data, which assists in assessing the instantaneous effects of creams on the skin more accurately.
In our experiments, we applied various types of creams to the skin surface and used terahertz imaging based on laser feedback interferometry to monitor real-time changes in skin hydration

By analyzing the imaging data, we assessed the differences in the moisturizing efficacy of different creams. In addition, to validate the accuracy of the terahertz imaging data, we used a conventional electrical method as a reference experiment. Comparison of the terahertz imaging results with the electrical measurements further confirmed the reliability of terahertz imaging in assessing the moisturizing efficacy of face creams.

In conclusion, terahertz imaging based on laser feedback interferometry shows great potential for assessing the effects of creams on the skin. Its high resolution and fast data acquisition capabilities provide detailed and accurate information about changes in skin hydration, which can contribute to the scientific evaluation and development of skin care products. This technology is expected to not only improve the efficiency of skin care product development but also provide consumers with more reliable verification of product efficiency.

Chapter 3. Literature review

3.1 Non-invasive technique to assess skin hydration

Over the past decades, scientists have developed several non-invasive methods to monitor skin function to investigate and predict skin barrier permeability. These techniques offer high precision and non-destructive advantages, allowing harmless research on the stratum corneum. In this paper, we will present electrical methods for in vivo evaluation of stratum corneum hydration, common medical imaging techniques, and terahertz-related techniques.

3.1.1 Electrical Methods

Techniques for assessing skin moisture based on changes in the electrical properties of the skin are extensively used in cosmetic and medical research. These methods infer the hydration level of the skin by measuring parameters such as electrical conductivity, impedance, or capacitance of the skin. In this article, two tools for evaluating skin hydration using the electrical capacitance and impedance methods will be presented.

1. Capacitance Methods

Corneometer CM 825

The Corneometer CM825 is a capacitance-measuring device that operates at 40-75 Hz and is sensitive to the relative dielectric constant of the material in contact with the probe [9]. The principle of keratometry is achieved by measuring the difference in the dielectric constant of the dielectric [10]. The dielectric constant of water differs from that of other substances. By measuring the change in capacitance of a dielectric (e.g. skin) in an electric field, it is possible to infer variations in its water content. Specifically, a change in the skin surface's hydration state leads to a modification in its dielectric constant, which in turn impacts the measured capacitance value. corneometer is popular because of its high reproducibility, ease of operation, short measurement time and low cost. Therefore, it is the instrument of choice for measuring the hydration level of the stratum corneum in experiments [11]. However, it is also sensitive to chemicals other than water on the skin surface [12]. Therefore, corneometer measurements cannot be considered purely as the water content of any substance they contact. The internal principal diagram and physical view of the CM825 are shown in Figures 1 and 2, respectively.

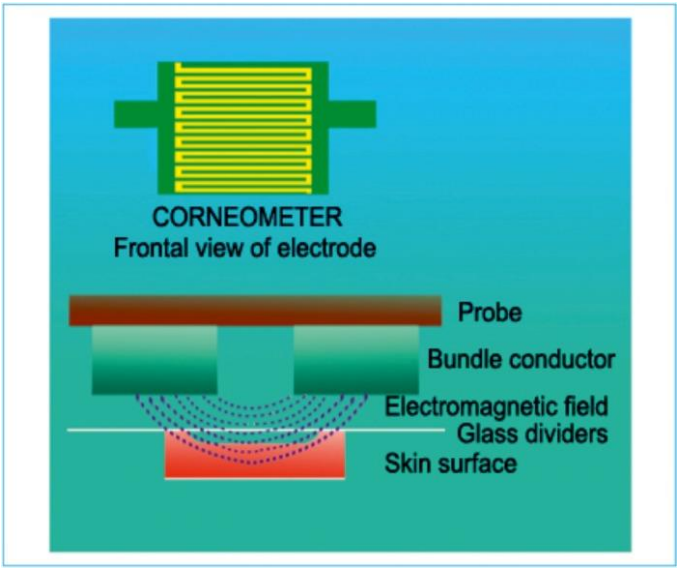

Figure 1. Probe structure of Corneometer

Source: Adapted from [10]

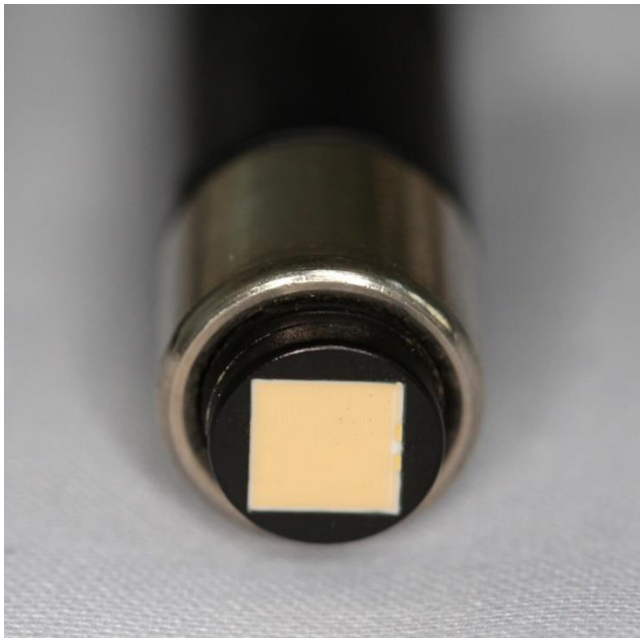

Figure 2. Probe graph of Corneometer CM825

Source: Adapted from [13]

2. Impedance Methods

Skicon 200EX

Skicon assesses the hydration status of the skin by measuring the conductivity of a single high-frequency current at a frequency of 3.5 MHz [14]. The instrument reads skin conductivity in microsiemens (μs), which has a range of 0 to 2000 μs [15]. The design of the probe uses large concentric fork-finger electrodes that are 75 μm wide with a gap of 200 μm between the electrodes (e.g. Figure 3). Also, the probe uses a spring system to apply a constant force of 0.78 N. This constant pressure assists in maintaining the consistency of the results and reduces measurement errors due to pressure variations. [16].

Figure 3. Probe graph of Skicon 200EX

Source: Adapted from [16]

In contrast to the Corneometer CM825, the Skicon 200EX is very sensitive to assessing conditions of extremely wet skin. It is not suitable for testing the stratum corneum of the skin in a low hydration state [16]. However, both require electrodes to be in contact with the skin during measurement, which may affect skin hydration. Moreover, both the Corneometer and the Skicon are affected to varying degrees by substances other than water, so they should not simply be regarded as a measurement of skin moisture content [12]

3.1.2 Medical Imaging Techniques

1. Magnetic resonance Imaging (MRI)

- Basic principle

Magnetic resonance imaging (MRI) can be a non-destructive technique to obtain the water content in the epidermis [17]. It is widely recognized as a very effective tool in measuring water content in the body and the movement of water through tissues [18]. When an MRI device is in operation, water molecules are exposed to a magnetic field and its protons interact with the external magnetic field. These protons absorb the external energy and perform a rotational motion after jumping from a low-energy state to a high-energy state, which results in the generation of a weak radiofrequency signal (RF). The coil in the device receives and converts these RF signals into images through computer algorithms. The eventually created picture demonstrates the distribution of water in various parts of the body, providing detailed information about the structure and water content of the tissue [19].

- Advantages and disadvantages

MRI high-resolution skin images clearly show the separate structures of the stratum corneum, epidermis and subcutaneous tissue [20]. It has been shown that MRI can be used to study the mechanisms of facial skin laxity through internal skin changes [21]. There are no longer any limitations to the extensive application of MRI imaging in dermatology and cosmetology [22]. However, MRI examinations usually require long acquisition times. The examined person must remain in a static state for a long period, sometimes close to an hour. The uncertainties associated with long scanning times can easily lead to scanning failures [23]. Furthermore, Although MRI is sensitive to water content and water structure in the body, it will struggle to achieve high sensitivity and resolution when applied to the study of dry stratum corneum [17].

- The figure of principle

Figure 4 presents the basic principle of the MRI.

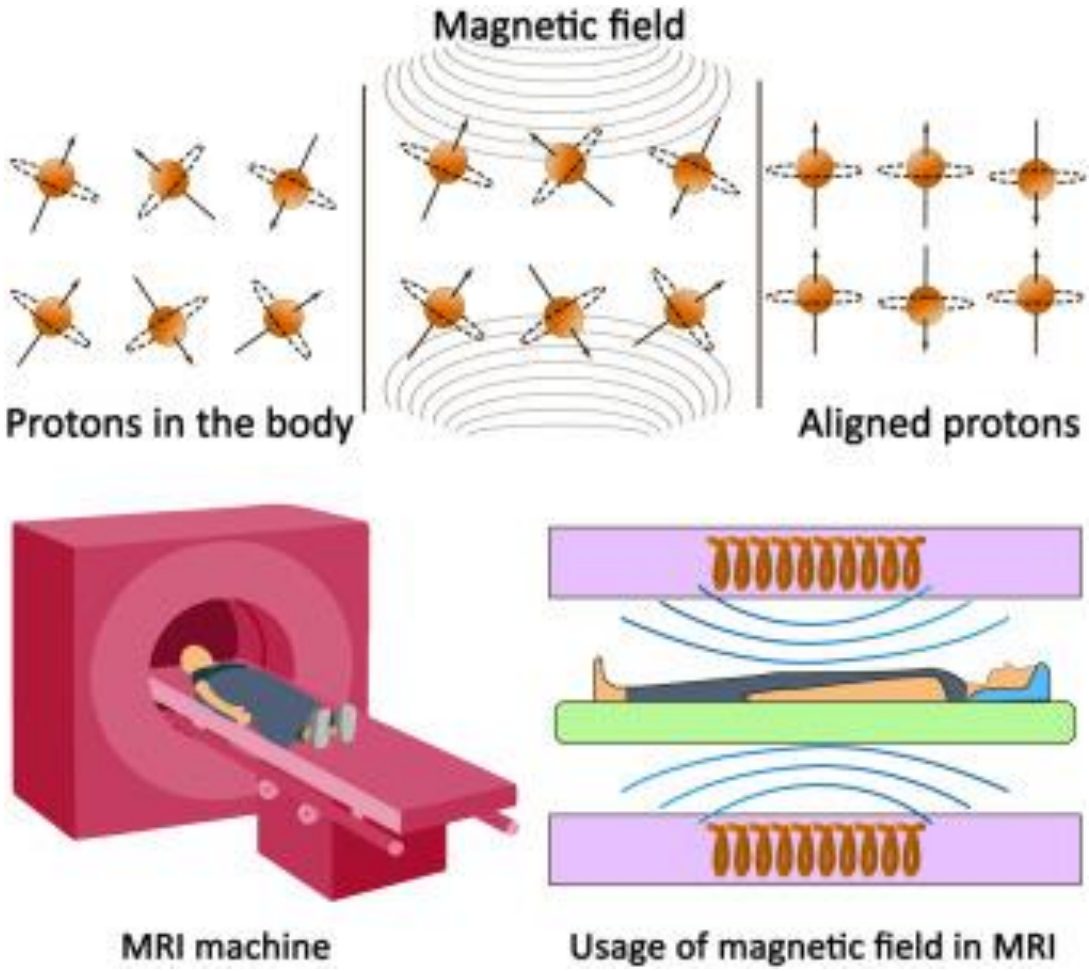

Figure 4. Basic principle of magnetic resonance imaging

Source: Adapted from [24]

2. Ultrasound

- Basic principle

Ultrasound is an imaging technique based on the emission and reflection of sound waves. Currently, a variety of ultrasound devices with variable frequencies are used to detect skin problems. It operates at frequencies ranging from 15 to 70 MHz and has a powerful capability to detect the type and velocity of blood flow [25]. When ultrasound penetrates the skin, it encounters interfaces of different densities and structures that reflect part of the sound waves. The structure of different tissues varies to some degree, resulting in their acoustic wave reflection coefficients being different. Therefore, the intensity and timing of the reflected waves will be used to generate an image of the internal structure of the tissue [26].

- Advantages and disadvantages

The depth at which sound waves penetrate the tissue varies with frequency. Low-frequency ultrasound is used to observe deeper structures, such as internal organs. High-frequency sound waves are more commonly used to look at proximal tissues to obtain clearer images of superficial structures [27]. For example, It can sensitively assess minor physiological changes in the skin [28]. Ultrasound not only enables noninvasive, real-time in vivo monitoring of hydration in various body parts but is also a relatively inexpensive method compared to other detection techniques [29].

- The figure of principle

Figure 5 briefly shows the basic principle of the ultrasonic machine.

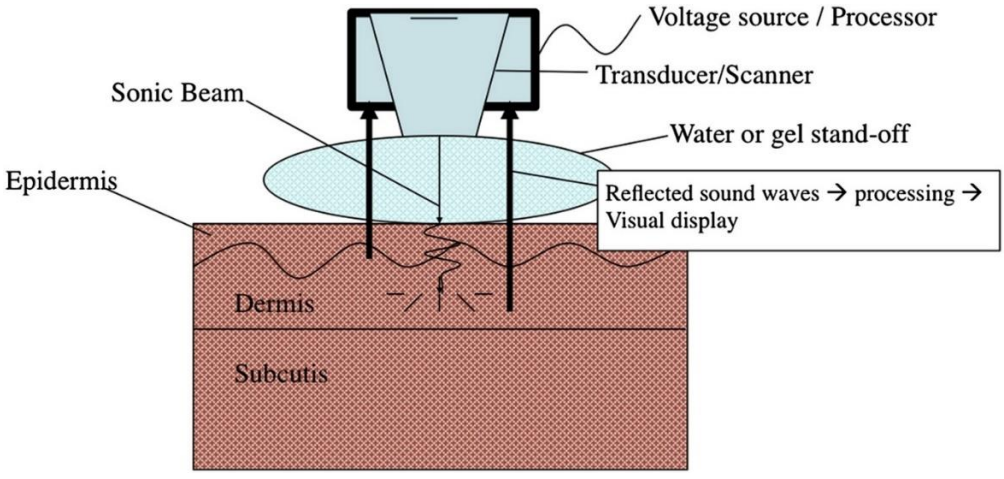

Figure 5. Depiction of ultrasound device

Source: Adapted from [27]

3.1.2 Terahertz-related Technique

- **Terahertz Time-Domain Spectroscopy (TDS).**

Terahertz Time-Domain Spectroscopy (TDS) is a technique for materials analysis and imaging using electromagnetic waves in the terahertz (THz) frequency range. Terahertz waves are generally referred to as electromagnetic waves with frequencies in the range of 0.1 to 10 THz. The TDS technique uses ultrashort terahertz pulses to obtain the physical and chemical properties of a sample by analyzing the behaviour of the pulses in the time domain [30].

- Basic principle

The following is the basic principle of TDS that I have summarized through [31].
Terahertz time-domain spectroscopy (THz-TDS) is a spectroscopic technique based on measuring terahertz electric fields in the time domain. Unlike conventional frequency-domain spectroscopy, THz-TDS directly measures the THz transient electric field rather than its intensity, providing detailed phase and amplitude information. Since terahertz pulses have very short durations (a few picoseconds) and the response times of direct electrical detectors and circuits are relatively slow, they cannot accurately capture and discriminate between these extremely fast-changing signals. This leads to measurements with insufficient time resolution to adequately reflect the transient characteristics of terahertz pulses.

To solve this problem, THz-TDS uses optical techniques to complete the detection. Femtosecond laser pulses (typically within 100 femtoseconds) are used to generate the terahertz pulses, while a part of the beam-split pulses is used as readout pulses for detecting the terahertz electric field during the detection process, and these pulses are very short. While the other part of the THz pulses is longer in the time domain and usually lasts for several picoseconds. The detector acquires a signal only when the readout pulse arrives at the same time as the THz pulse. To obtain the time evolution of the entire THz pulse, the TDS adjusts the relative arrival times of the read-out pulse and the THz pulse by using a mechanical delay line.

- The figure of principle

Figure 5 shows a simplified THz time-domain spectrometer (THz-TDS). The femtosecond laser pulse output is divided into two beams by a beam splitter (BS). One beam is utilized to produce the THz radiation, while the other beam of light travels through a delay line and is employed to detect the terahertz beams.

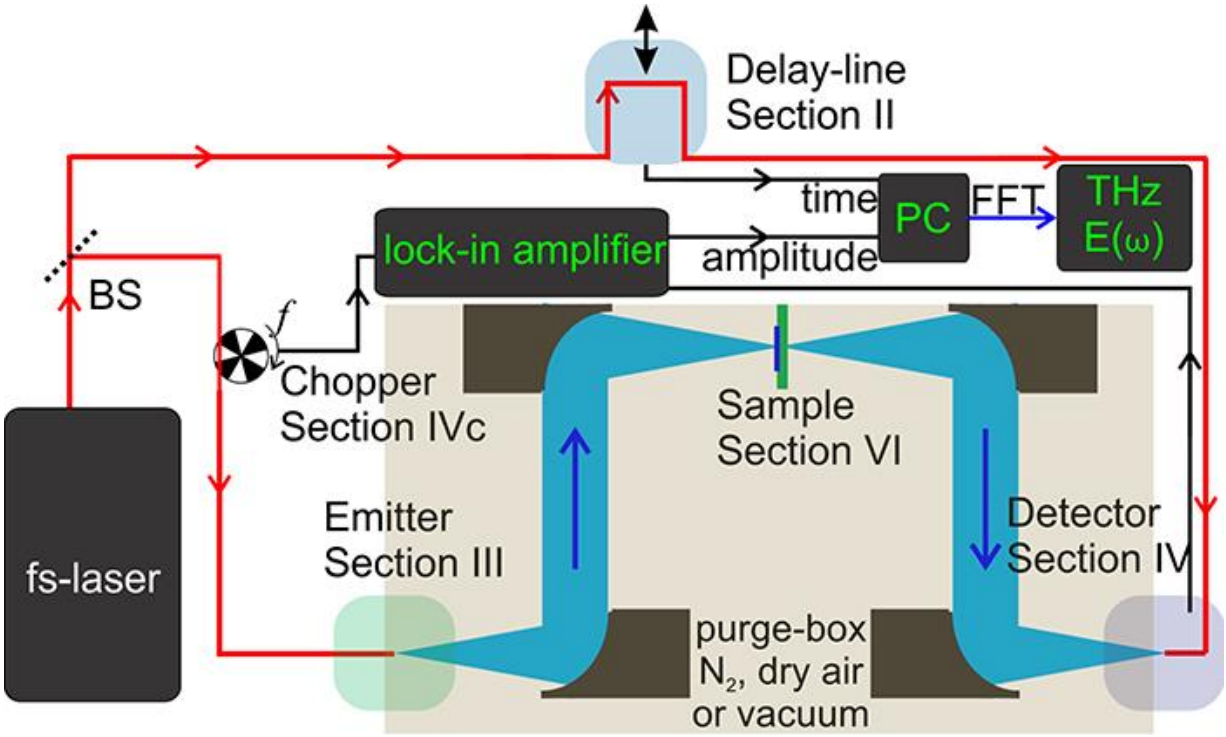

Figure 6. Simplified THz time-domain spectrometer

Source: Adapted from [31]

- Advantages

TDS plays an essential role in the study of living tissues in terms of high sensitivity and non-ionization in water [32]. For in vivo studies, it can be used to detect early diabetic foot syndromes and is of significant assistance in the prevention and treatment of foot complications in diabetic patients [33]. In addition to this, it can be used to observe subtle changes in scars, effectively improving scar treatment and management issues [34]. TDS has been reported to be used to demonstrate the effect of different moisturizing substances on the stratum corneum [5]. Variable frequency terahertz was used to determine the water content of the skin. The authors of the experiments suggest that the results can be judged and summarized by observing terahertz TDS imaging, which is an essential research technique in the field of medicine and biology.

- Disadvantages

However, TDS produces a terahertz spectrum with an extremely large bandwidth, resulting in a small terahertz field amplitude. Although the power of the femtosecond laser can be increased to achieve a larger terahertz field amplitude. However, this requires large, complex, and expensive system setups to accomplish [35]. In addition to this, it has a slow image acquisition rate [36], and the uncontrolled loss of easily evaporated material during the experiment may lead to an increased difference between the experimental and actual results.

Chapter 4. Terahertz Quantum Cascade Lasers (QCL)

4.1 Introduction

In 1971, Esaki and Tsu first introduced the idea of radiative amplification using " inter-subband transitions", which became the core concept for the subsequent development of QCL [37]. In 1994, quantum cascade lasers were proposed and demonstrated by Faist J et al [38]. After decades of exploration by scientists, it has rapidly evolved from a laboratory principle to a powerful and groundbreaking technology.

Terahertz radiation enables safe detection by imaging weapons, drugs and explosives [39]. Compared to microwaves, terahertz radiation provides better spatial resolution due to its shorter wavelength. In addition, terahertz imaging is non-invasive, safer and more harmless than high-energy X-ray imaging [40]. Moreover, many molecules and solids exhibit strong and unique spectral features due to the wide variation of absorption and refractive indices of different materials in the terahertz spectrum [41]. Thus, it provides better contrast in recognizing different materials. However, the terahertz region of the electromagnetic spectrum was initially underdeveloped because of the lack of low-cost, efficient techniques for generating coherent THz sources. The appearance of THz quantum cascade lasers (QCLs) provided the solution [42]. Figure 7 presents the timeline of Quantum Cascade Laser (QCL) Technology Innovation [43].

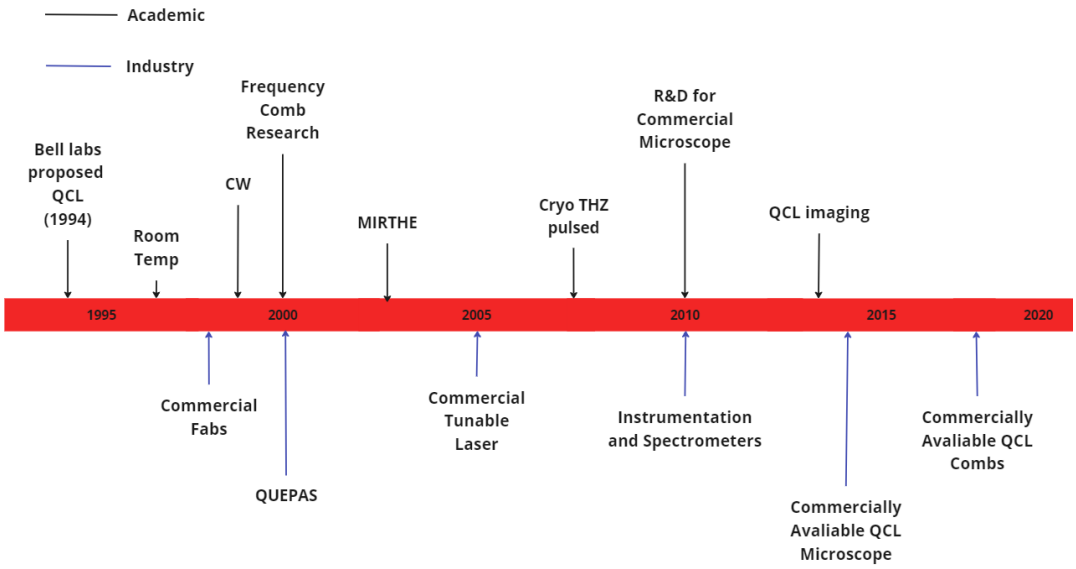

Figure 7. Timeline of Quantum Cascade Laser (QCL) Technology Innovation

4.1 Laser Feedback Interferometry

One of the most basic coherence techniques is laser feedback interferometry. It is also known as self-mixing interferometry (SM). The combination of QCL and LFI provides a high-speed, high-sensitivity detection mechanism in the THz band for sensing applications [44]. LFI with QCL has been demonstrated for various applications including materials analysis, biomedical imaging, and near-field imaging [45].
Here is the basic principle and simple schematic of LFI.

Basic principles of the LFI system:

1. Light is emitted from the laser.
2. The emitted radiation interacts with and is partially reflected on the external target.
3. A portion of the laser light then returns to the laser cavity. The parameters of the laser will be changing. This is due to the mixing of the reflected radiation with the electric field in the cavity.

Figure 8 is a simple LFI three-mirror laser model to show the LFI architecture.

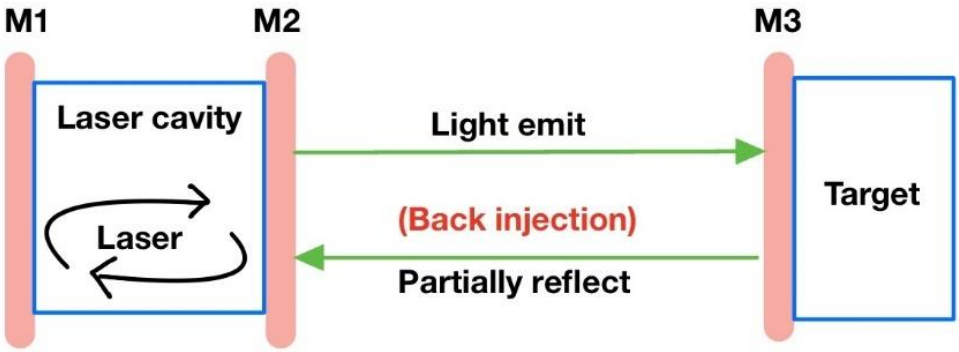

Figure 8. LFI three-mirror laser model

4.2 Terahertz QCL for Biological Imaging

After the first practical demonstration of terahertz imaging, the technique aroused great interest among researchers. Until now, imaging with terahertz radiation has been used in various industries. Since terahertz radiation is in the category of non-ionizing radiation, the energy of photons in its spectral region is relatively weak. As a result, molecules in water tend to collide with each other in this region [46]. This provides a convenient tool for the biomedical field.

Unlike Thz-TDS imaging reported in many bioimaging studies, QCL power is many orders of magnitude higher than typical time-domain systems and has the advantage of fast data collection [47]. It has become the preferred stable high-power light source in laboratories, radiating at frequencies typically between 1 and 5 terahertz [48]. The QCL technique has been demonstrated to be useful for imaging tissue samples. As mentioned in Yah's article, terahertz QCL at 2.59 THz was used for coherent imaging of pig tissue samples [49]. Juraj et al. also used an imaging system with a terahertz QCL with a frequency of 3.45 THz on brain tissue samples, achieving a resolution close to the diffraction limit and a dynamic range of 1000 [50]. Biomedical imaging of small mammalian brain slices and metastatic liver tissue using terahertz QCL runs at 3.7 terahertz and derives their structural contrast through differential absorption of terahertz radiation. These were proposed by researcher Seongsin et al [51].

4.4 Potential Interference Factors

Terahertz decays in the skin because of the high water absorption, so most experimental setups for human skin measurements are performed with reflective geometries. Among these, quartz windows are the preferred material to be used as an assistant for the experiments [52]. The effect of masking has also been suggested by Sun et al. Their results show that the terahertz response is also affected during the first five seconds of contact with the window. And the longer the occlusion time, the terahertz pulse amplitude will be reduced [53]. Therefore, before determining the terahertz imaging experiments, it is necessary to develop experimental protocols and processing techniques to avoid too many uncertain variables having a large impact on the experimental results.

Chapter 5. Research Plan

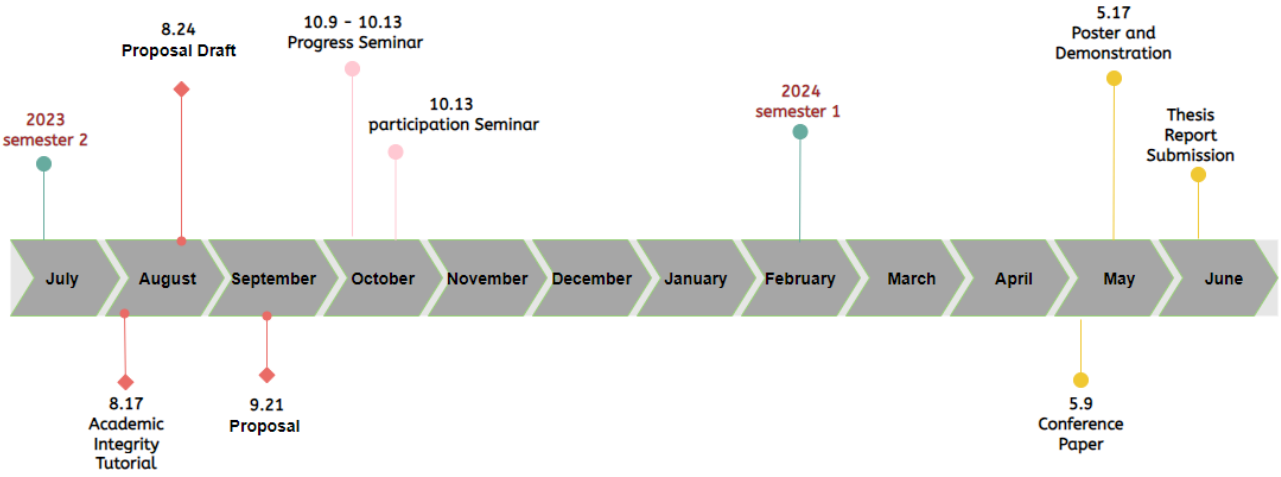

Figure 9. Project Plan with Timeline

5.1 Milestones

Milestone 1: Preliminary Research

Duration: 31/07/2023 – 21/09/2023

This milestone mainly provides basic information for my project by reading past research and literature reviews. This period is to adjust and determine the final research direction after the preliminary research on the project. Academic Integrity Modules and Project Proposals should be completed at this milestone, as indicated by the assessment tasks highlighted in red in Figure 9.

Milestone 2: Experimental design

Duration: 22/09/2023 – 13/10/2023

This milestone is mainly to interview the supervisor, understand the specific content of the experiment and conduct preliminary experimental design. The basic knowledge required for reading and understanding the project. At this milestone, students attend seminars to give an oral presentation of the main content of their research and work in progress. Just like the tasks shown by the pink symbols in Figure 9.

Milestone 3: Doing experiments and obtaining data

Duration: 14/10/2023 – 21/03/2023

This milestone takes the longest and is the most cumbersome. It involves doing experiments and processing the data after it is obtained. After improving and changing the experiment, the most accurate data results are finally obtained.

Milestone 4: graduation thesis writing

Duration: 22/02/2023 – 03/06/2023

This milestone is mainly to summarize the experimental results. In addition to completing a conference paper, it is also necessary to make a poster for the graduation thesis and complete the final graduation thesis, as demonstrated by the yellow symbols in Figure 9.

Chapter 6. Methodology

This section will cover the design process of traditional electrical methods (corneometer CM825) and terahertz QCL experiments. The materials and facility setup involved in the experiments will be demonstrated.

6.1 Experiment Preparation

(1) *Experiment participants*:

Experimenters have been told to understand the relevant regulations of the experiment and voluntarily participate in the experiment. Since the experimenter is the proposer of this project, this project does not require an application for relevant ethical approval.

(2) *Experimental materials*

1) Two different ***creams*** were used in this experiment:

- **L'Oreal** Day cream.
- **L'Oreal** Eye Cream.

Figure 10. L'Oreal Creams pictures.

(a) L'Oreal day Cream. (b) L'Oreal eye cream.

2) lab alcohol, aluminum paper sheets with three equal-sized 1*1cm square windows, sterile spatula, cotton swab, tissue paper

(3) ***Experimental instruments:*** Terahertz QCL transmitter device, Corneometer CM825, 2-inch diameter round plastic and its support frame

6.2 Thz-QCL Experiment with LFI

Our THz QCL device emits a single frequency of around 2.8 THz. In our experiments, we use a terahertz imaging technique based on laser feedback interferometry to monitor real-time changes in skin hydration. The following is the simplest description of our QCL imaging experiments incorporating the working principle of LFI. The simple model setup of our QCL is illustrated in Figure 10.

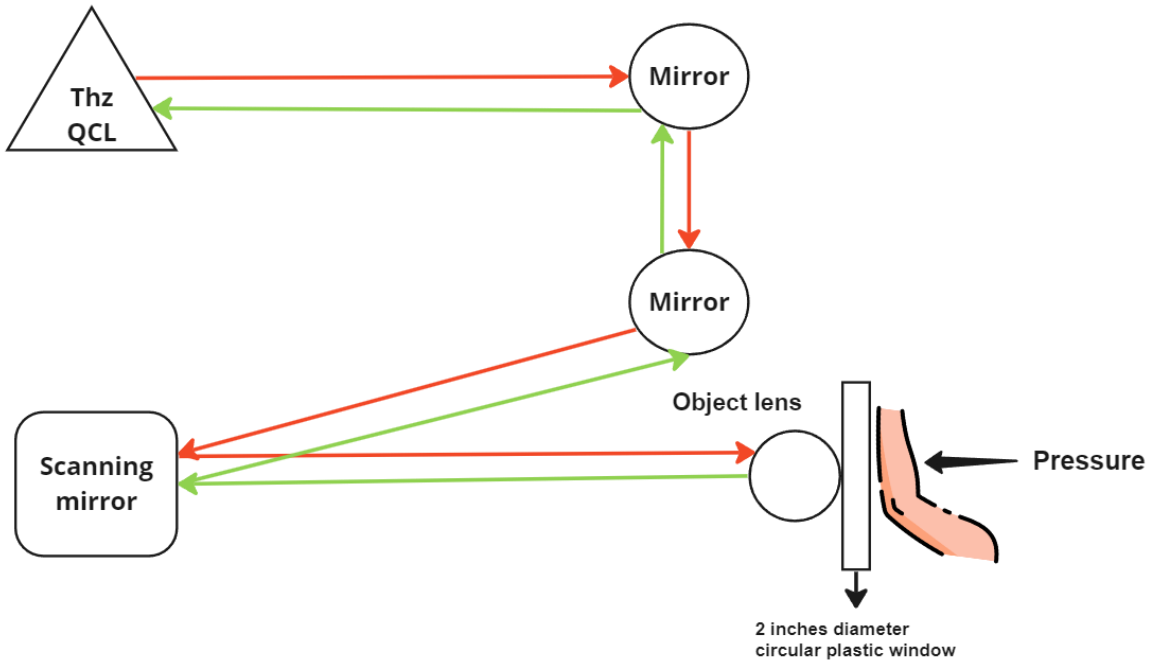

Figure 11. QCL model

- **LFI process for QCL experiment**

- **Laser emission process (red line)**

I. The laser beam emitted by the QCL is collimated through a collimating lens.
II. Then guided to the scanning mirror through two mirrors.
III. Passes through the objective lens and onto the arm.

- **Laser reflection process (green line)**

I. The laser reflects into the laser cavity from each skin pixel.

II. Mixes with the intra-cavity electric field and generates a self-mixing (SM) signal in the terminal voltage of the laser.

III. Fourier transform converts the time-domain SM signal into the corresponding amplitude and phase at different SM waveform frequencies.

IV. These amplitude and phase at each pixel of a skin were used to create the THz amplitude and phase images, respectively.

6.3 Original Experiment

6.3.1 Experiment Procedure

Use a cotton swab soaked in alcohol to cleanse the skin's surface and allow the alcohol to evaporate completely. Utilize the double-sided tape to affix aluminum foil sheets to the inner skin of the corresponding area on both arms. A sterile spatula was used to evenly apply each cream to a thickness of approximately 0.1mm onto the corresponding area of the arm. The application areas on both arms, from top to bottom, are as follows: eye cream, reference group, and day cream. Among them, the reference group did not apply any cream. Figure 13 shows the shape of the aluminum paper sheets on the arms and the distribution of the three areas. After waiting for 30 minutes, the skin of the left arm will be measured using CM825, while the terahertz QCL system will be used to measure the skin of the right arm. Two experiments were performed simultaneously. The intervals between arm tests were 10 minutes, and the experiment was performed 6 times, with a total duration of 80 minutes. Figure 12 shows the flow chart of the entire experimental operation.

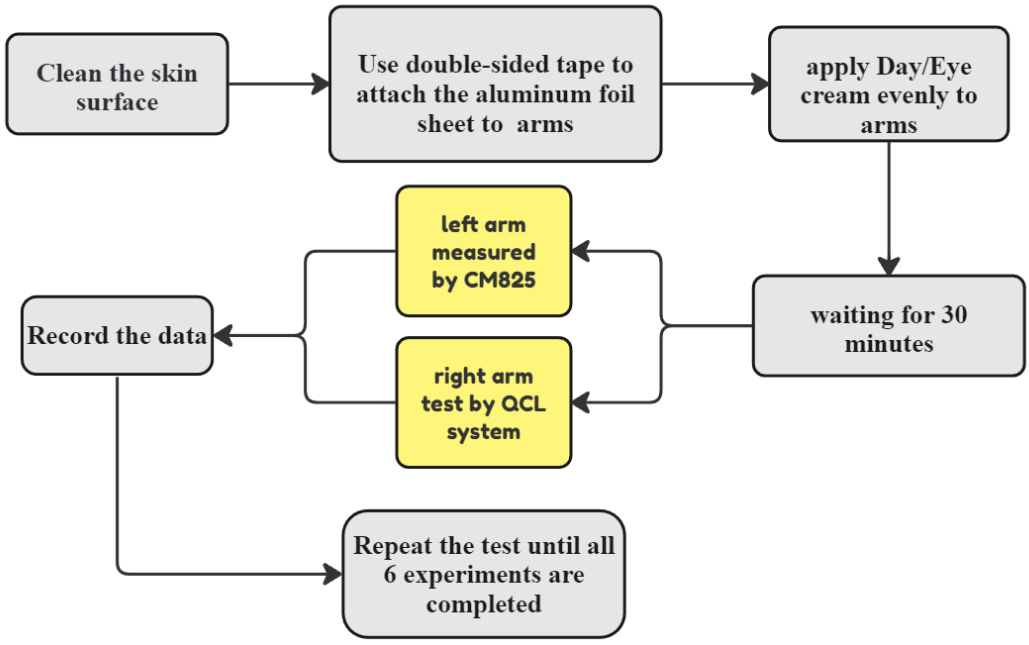

Figure 12. Flow chart of the experimental operation

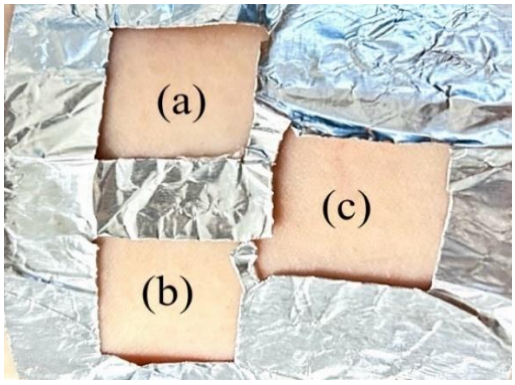

Figure 13. Aluminium paper sheets on the arms.

(a) L'Oréal eye cream. (b) L'Oréal day cream (c) reference group.

(1) Corneometer CM825 experiment details

Use the probe to press each area of skin, generate data and release the probe. When measuring different areas, wipe the probe with a tissue so that cream residue does not affect other areas. Apply 20 presses to each area.

(2) THz - QCL Experiment details

Measurements with the QCL were taken with the skin pressed against a 2-inch diameter circular plastic window. Each scan lasted approximately 2 minutes, and the measurement was terminated when the arm image was displayed on the screen after a complete scan. The system does not stop scanning between each test, so data needs to be manually saved after each arm scan.

6.3.2 Data Analysis

- **THz - QCL Experiment**

The QCL system outputs data as HDF5 files containing amplitude data for each scan. The data is stored in the form of a matrix, where each element of the matrix represents the amplitude value of a pixel of the skin on a two-dimensional plane. This experiment stores a total of 6 sets of experimental data. The size of each matrix is 400 *1400.

i. Visualization data:

After the Fourier transform, we get the amplitude of each pixel of the skin, so the overall image of the arm amplitude can be drawn. Use the surf function to create a 3D surface plot that shows the distribution of amplitudes on a two-dimensional plane. Select the surface shading mode to 'flat' and set the color map to HSV color mode with 256 colors. This will reflect the differences in amplitude of the various regions through the colors. Figures 14 to 19 show the amplitude images of 6 groups of tests.

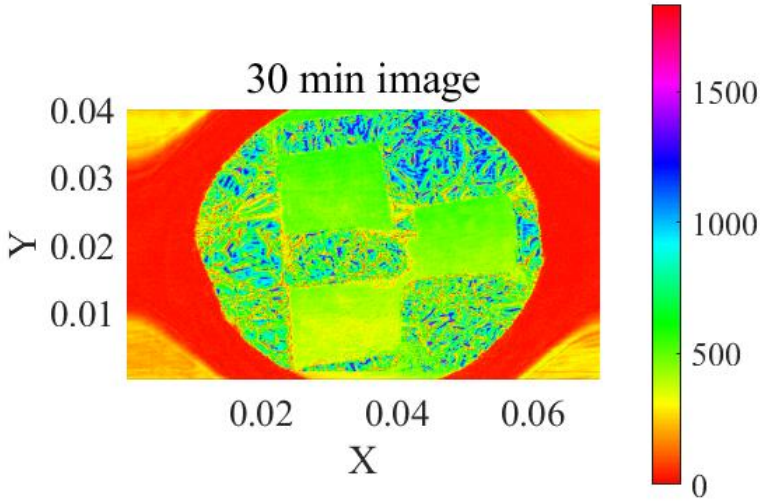

Figure 14. Amplitude images of 30 minutes

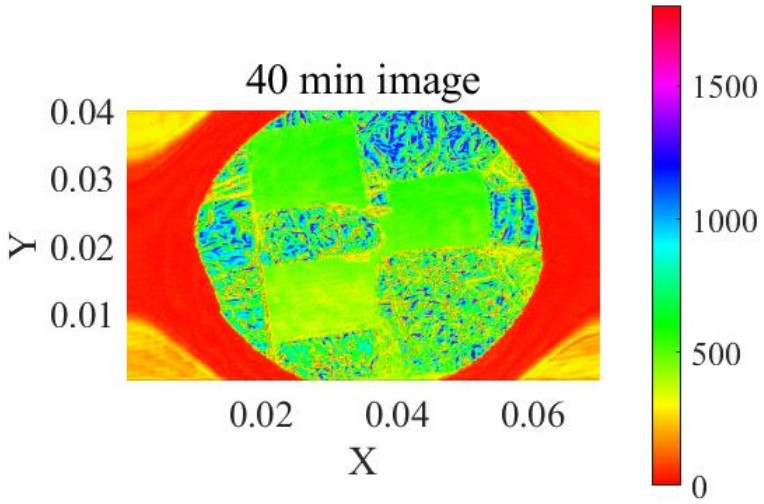

Figure 15. Amplitude images of 40 minutes

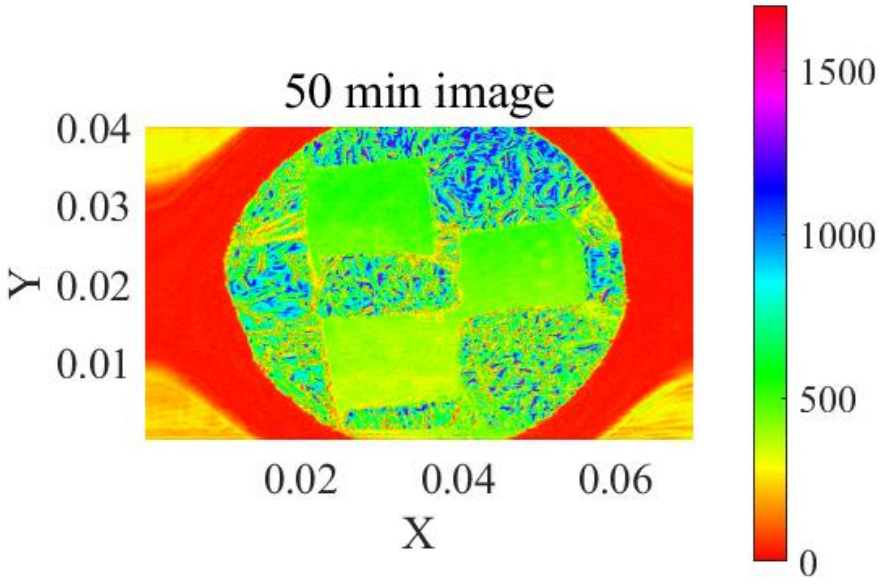

Figure 16. Amplitude images of 50 minutes

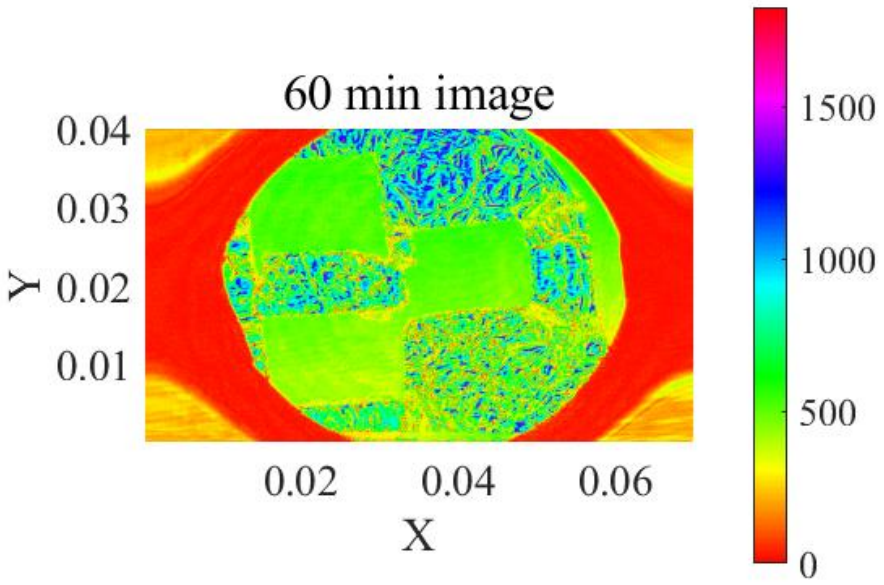

Figure 17. Amplitude images of 60 minutes

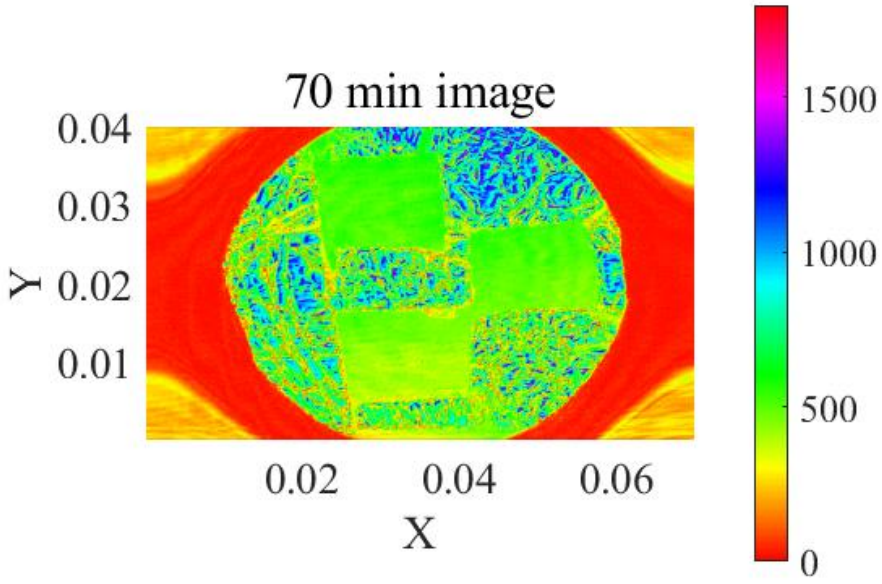

Figure 18. Amplitude images of 70 minutes

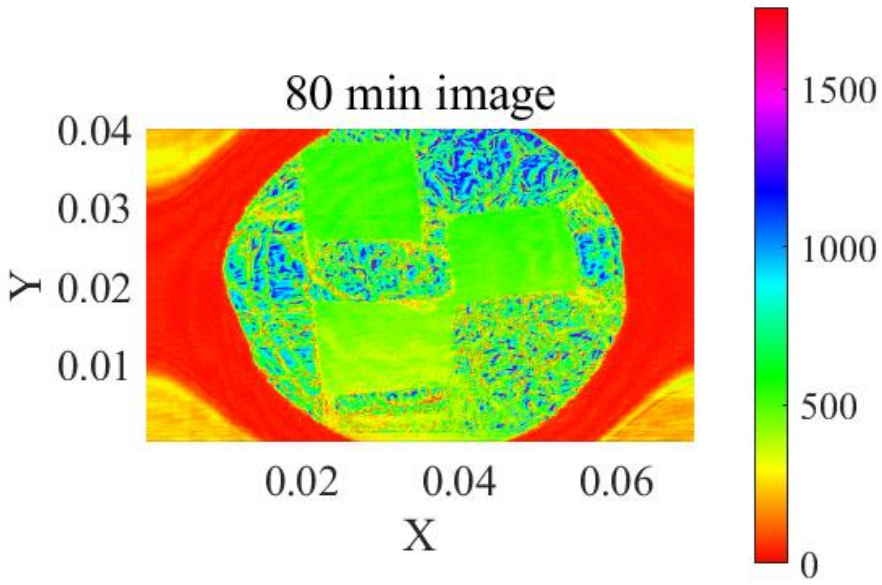

Figure 19. Amplitude images of 80 minutes

ii. Processing data

Firstly, a matrix range of 60*200 is selected in each of the three regions. Since the placement of the arm is different for each test (as shown in Figures 14 to 19). To ensure that the selected region is within the valid range each time, the matrix coordinates shown in the picture need to be manually adjusted. Once the three sets of ranges were determined, the mean function was utilized to calculate the average of all points within these ranges. All six sets of data were processed to generate a graph depicting the average amplitude and time of the three regions over 50 minutes. Figure 20 shows the results for the three groups of regions. We still performed normalization processing to see the trend of day cream and eye cream in eliminating environmental impact. Figure 21 shows the data after dividing the average value of eye and day cream by the reference group respectively.

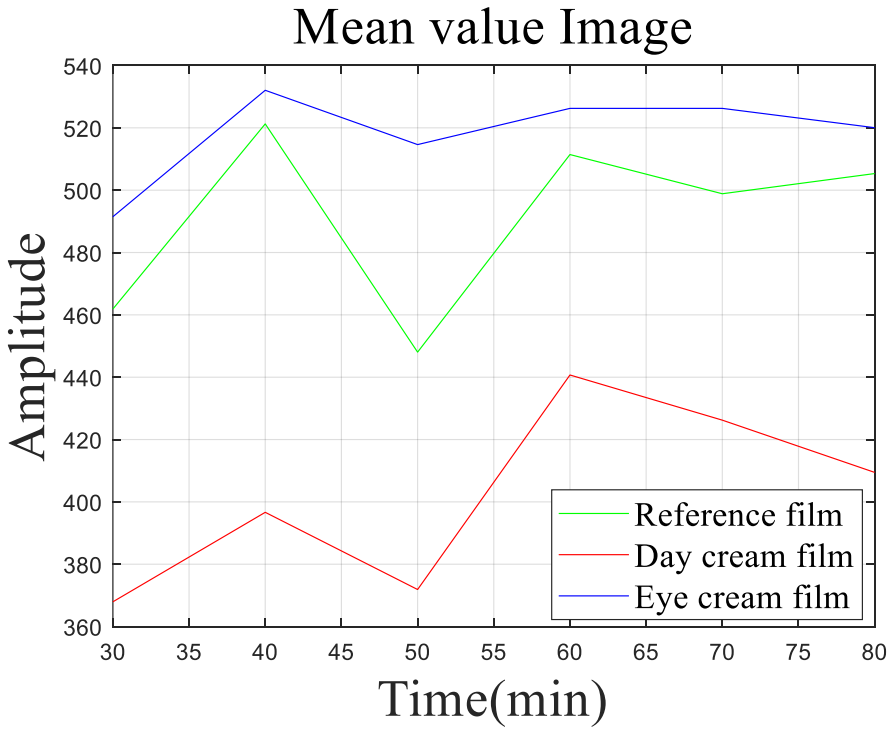

Figure 20. Mean value image of the original Thz experiment.

(red line) L'Oreal day cream. (blue line) L'Oreal eye cream. (green line) reference group.

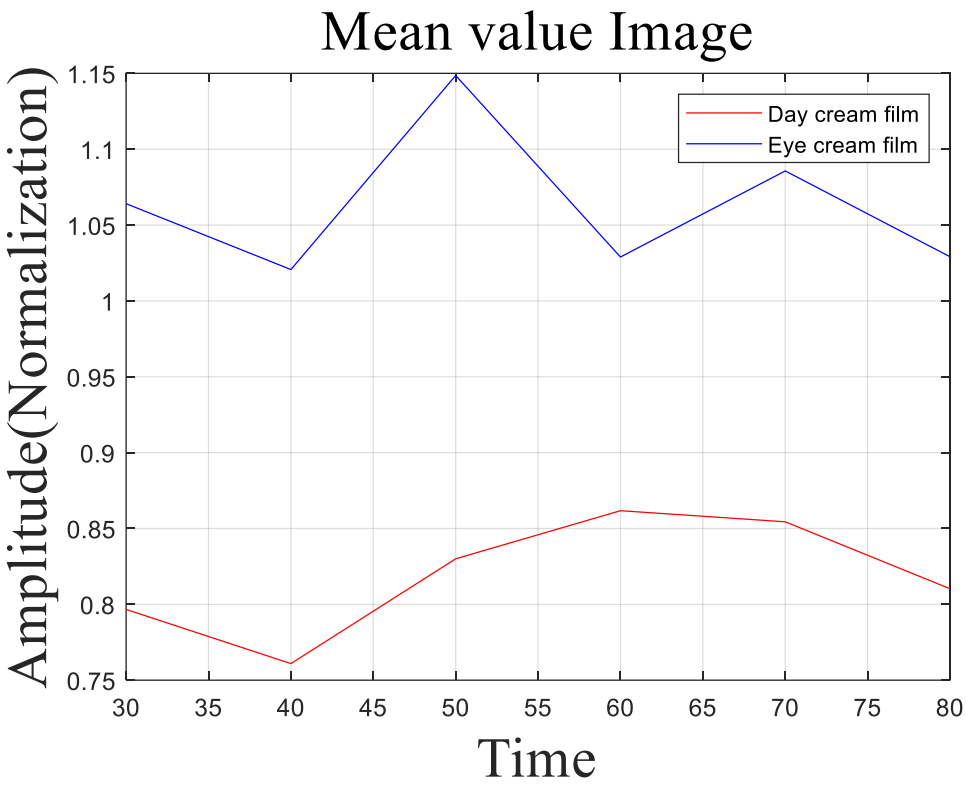

Figure 21. Normalisation value image of the original Thz experiment.

(red line) L'Oréal day cream. (blue line) L'Oréal eye cream

iii. Analyzing data

As shown in Figure 20, the curve of the reference group consistently falls between that of the eye cream and the day cream. This suggests that the skin of the reference group (without any cream applied) is moister than the skin to which the eye cream was applied. Theoretically, this phenomenon is impossible for skin with normal absorption function. After analyzing the corneometer CM825 data, it was found that, as shown in Figure 22, the moisture content of the reference area should always be lower than that of the day cream and eye cream areas. Therefore, there are some issues with our QCl experimental design.

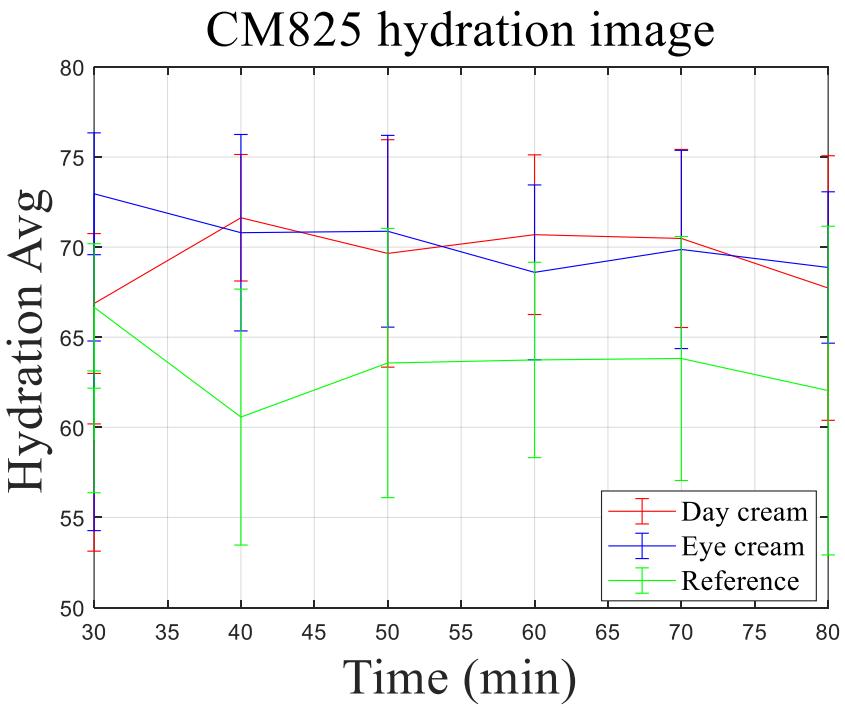

Figure 22. CM825 hydration image of the original experiment.

(red line) L'Oreal day cream. (blue line) L'Oreal eye cream. (green line) reference group.

6.3.3 Discussion

We speculated that the issue primarily arose because the three areas were not on the same horizontal plane. The skin on the arm forms a curved surface. When pressure is applied to this curved surface, the pressure distribution may become uneven due to the geometric shape of the curve. In the experiment, the eye cream area was located near the top by the window. When most of the applied pressure was concentrated on the middle and lower parts, the day cream and reference areas received more pressure than the eye cream area. This hypothesis is substantiated by the existing literature [54]. The article concludes that as pressure on the skin increases, reflectivity decreases across all frequencies, resulting in a decline in signal amplitude. Therefore, when the eye cream area is subjected to less pressure, its reflectivity rises. As a result, its curve ends up showing a greater amplitude than that of the reference area.

To better analyze the hydration effect of different creams on the skin by terahertz QCL, we modified the experimental settings and plans and conducted the experiment again.

6.4 Final Experiment

6.4.1 Experiment Procedure

After cleaning the skin surface, aluminum foil sheets with three areas at the same level were attached to the inner skin of the corresponding areas of both arms using double-sided tape. Figure 24 shows the shape of the new aluminum paper sheet. The application areas on both arms, from left to right, are as follows: eye cream, reference group, and day cream. After waiting for 10 minutes, the skin of the left arm will be measured using CM825, while the terahertz QCL system will be used to measure the skin of the right arm. The intervals between each test are 10 minutes, for a total of 100 minutes. Figure 23 shows the flow chart of the entire new experimental operation.

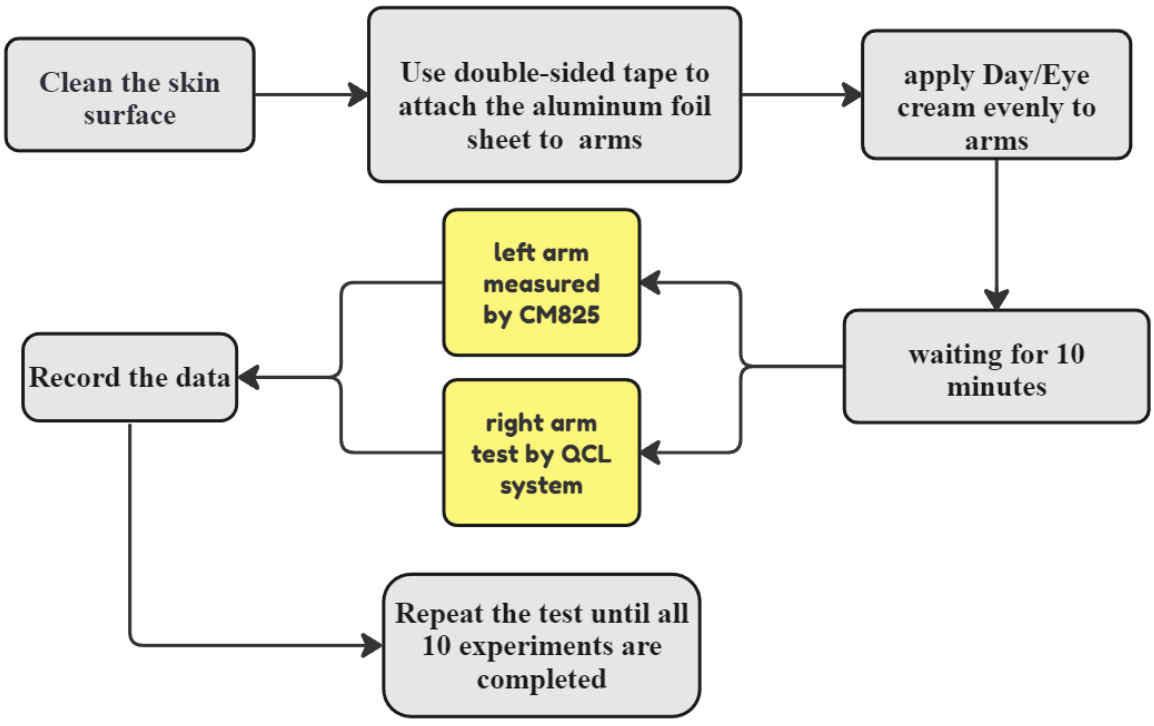

Figure 23. Flow chart of the final experimental operation

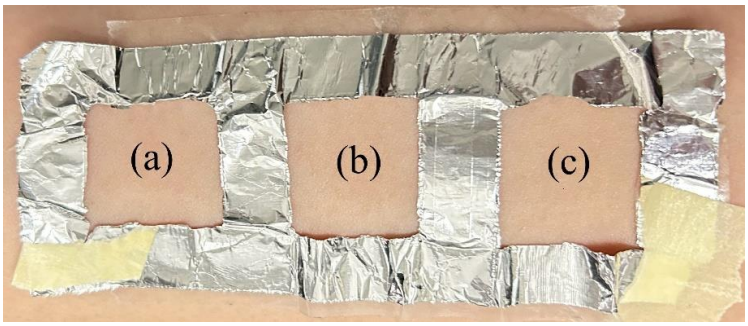

Figure 24. Aluminium paper sheets on the arms.

(a) L'Oréal eye cream. (b) reference group. (c) L'Oréal day cream.

(2) Corneometer CM825 experiment details

Still using the probe, apply pressure to each area of the skin. Apply 20 compressions to each part.

(2) THz - QCL Experiment details

Measurements were taken with the QCL while the skin was still pressed against a 2-inch-diameter circular plastic window. The new QCL experimental system continuously scans and automatically saves all data between each test. This also includes background data without arms.

6.4.2 Result & Data Analysis

- **THz - QCL Experiment**

There are 82 sets of data in the new QCL experiment, still stored in the form of a 400*1400 matrix. The amplitude values of each pixel were transformed to produce 82 consecutive images. Ten of them contained images of the arm and the rest were blank background pictures.

i. Visualization data:

Upon observing the amplitude images of the ten test groups, we noticed the occurrence of ring curves that were not present in the previous experiments. Therefore, we chose to inspect the blank images that preceded these ten sets of data. The results showed that all ten sets of blank images contained Newton's rings.

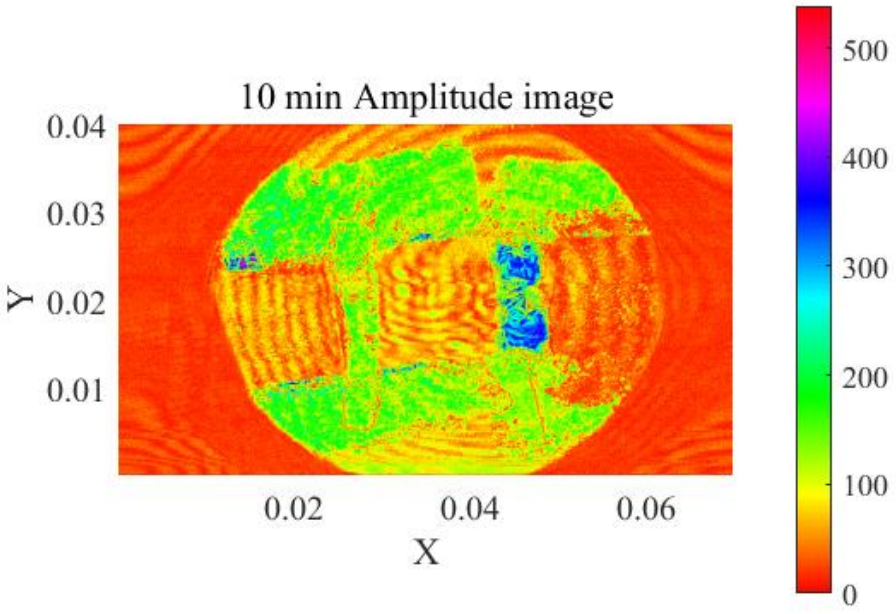

Figure 25. Amplitude image of 10 minutes

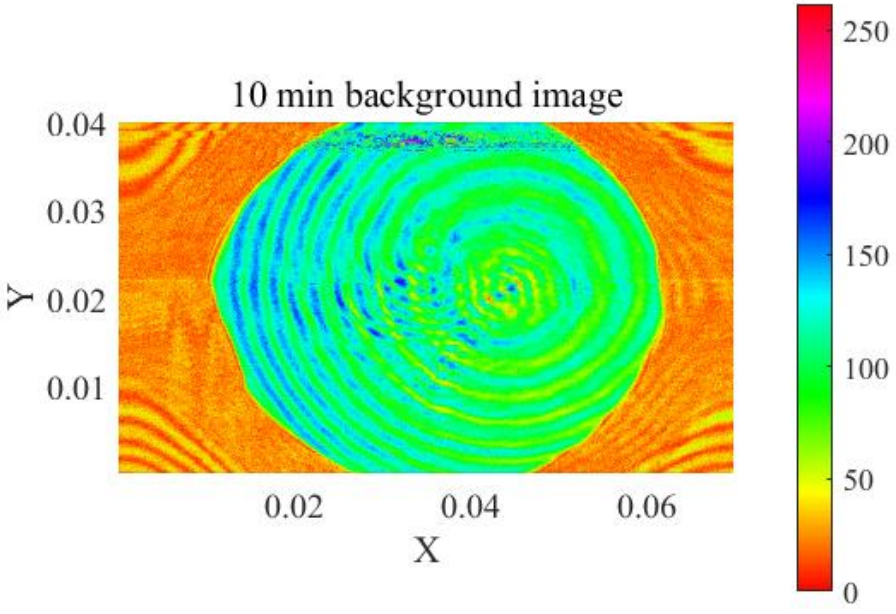

Figure 26. Background image of 10 minutes

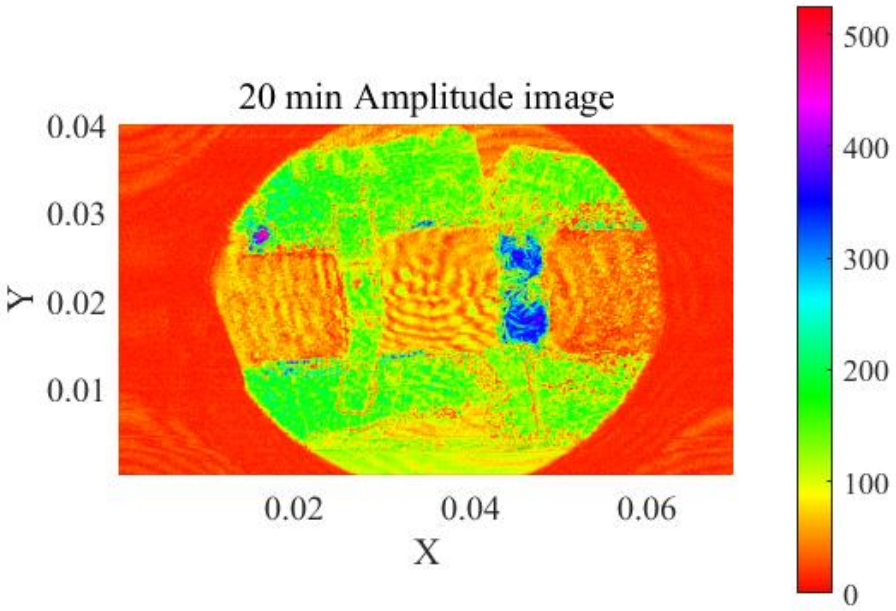

Figure 27. Amplitude image of 20 minutes

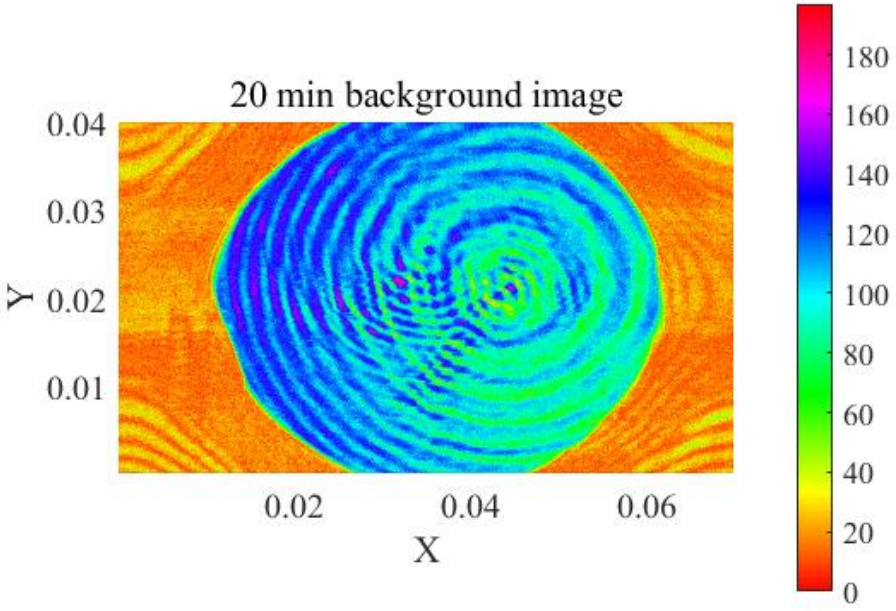

Figure 28. Background image of 20 minutes

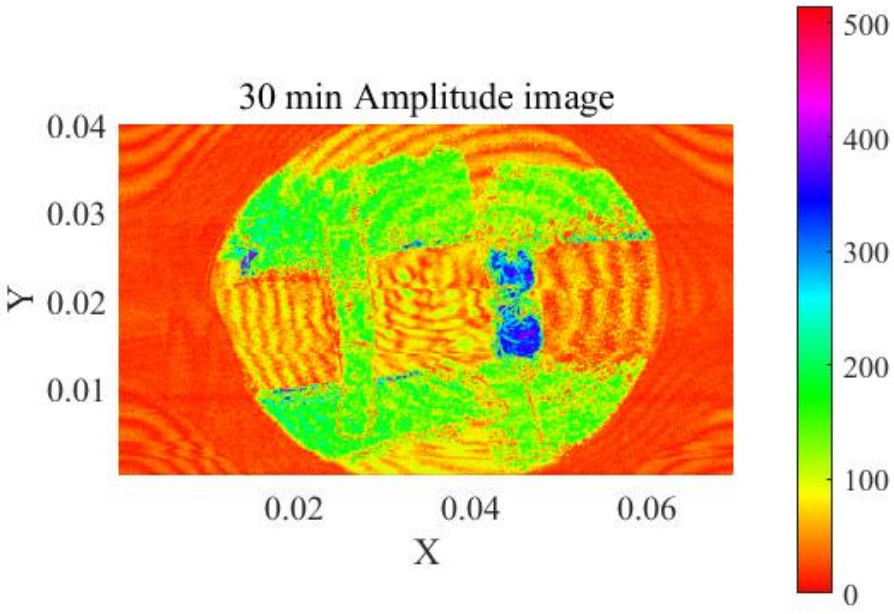

Figure 29. Amplitude images of 30 minutes

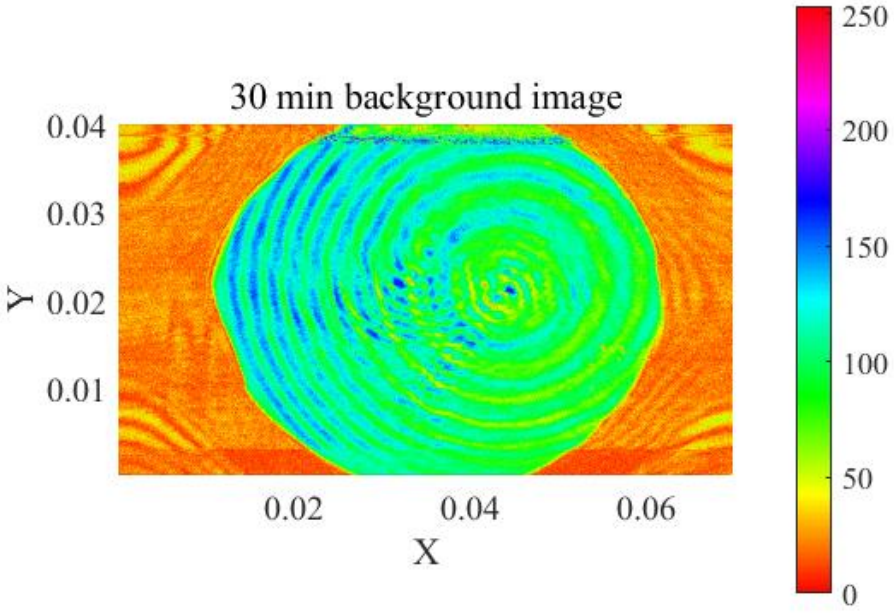

Figure 30. Background image of 30 minutes

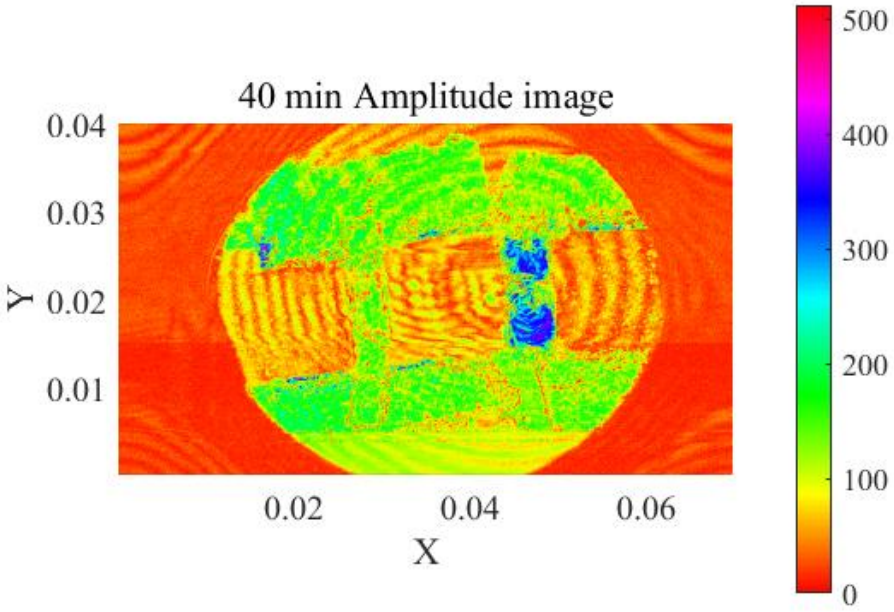

Figure 31. Amplitude image of 40 minutes

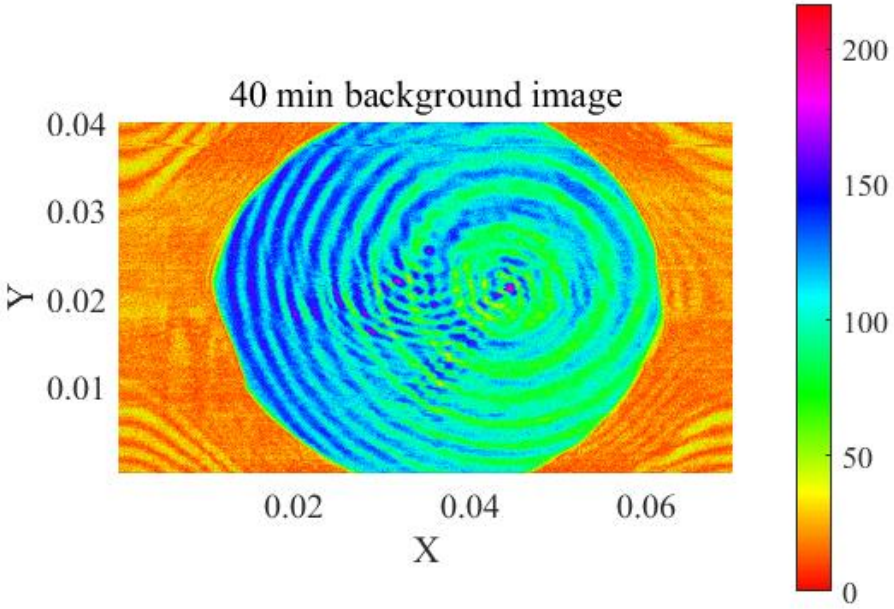

Figure 32. Background image of 40 minutes

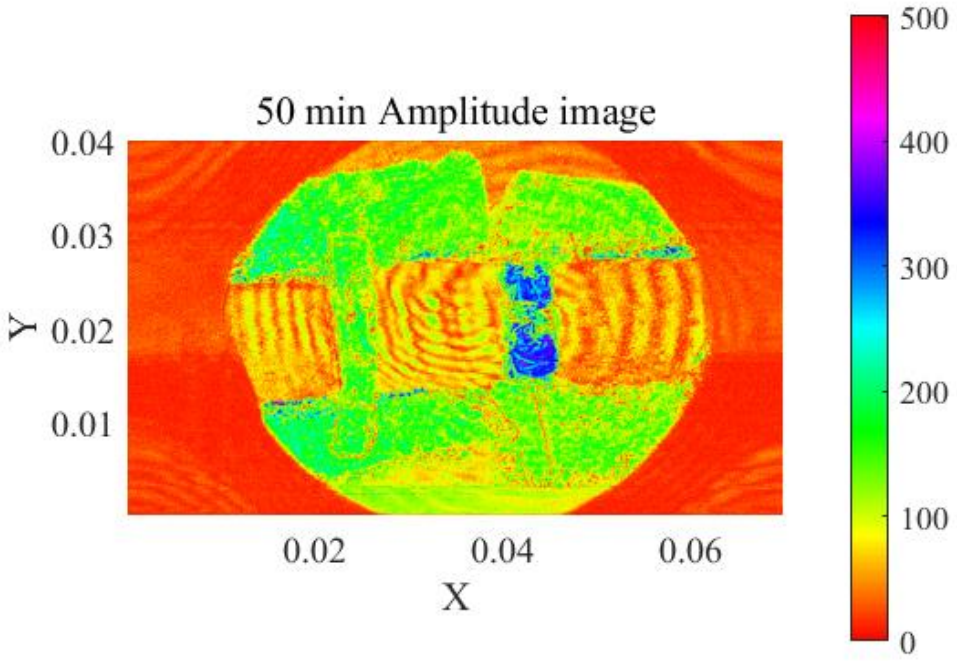

Figure 33. Amplitude image of 50 minutes

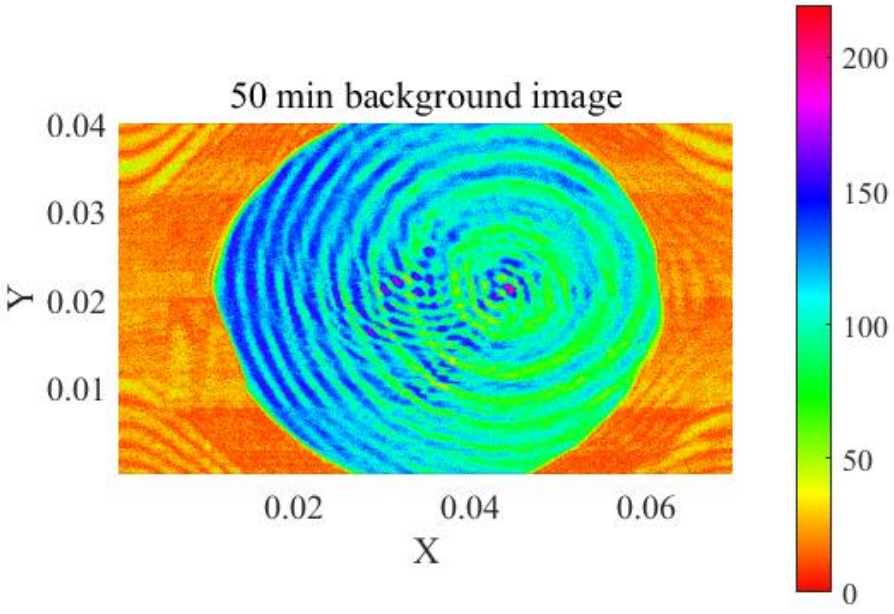

Figure 34. Background image of 50 minutes

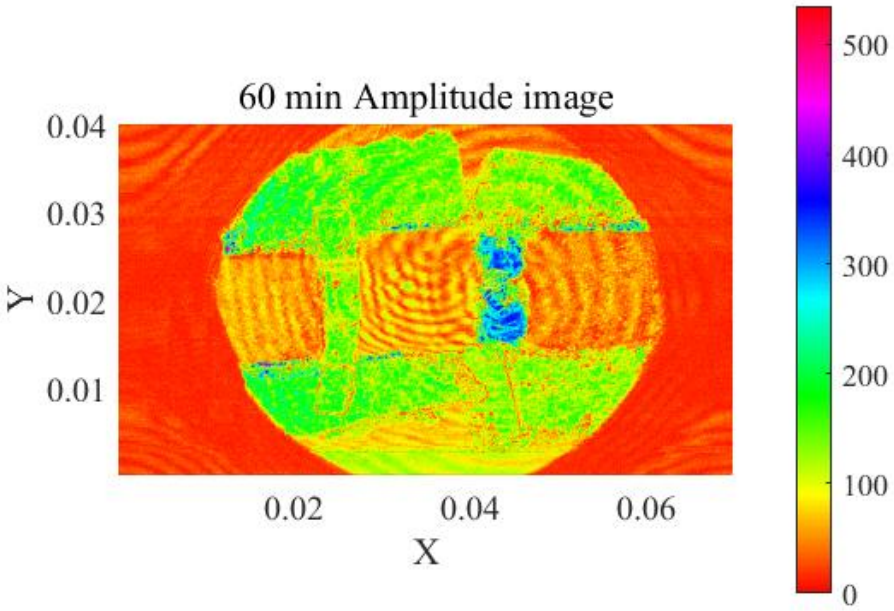

Figure 35. Amplitude image of 60 minutes

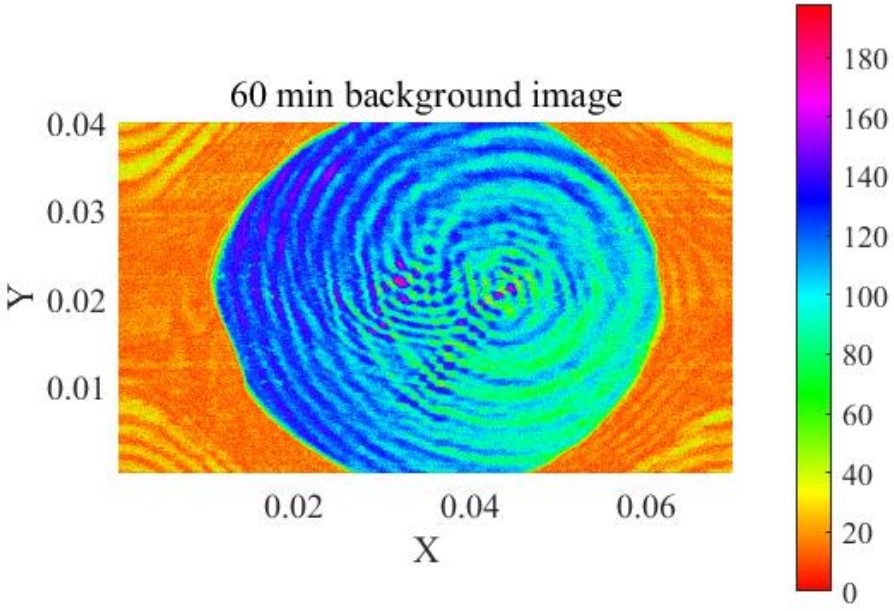

Figure 36. Background image of 60 minutes

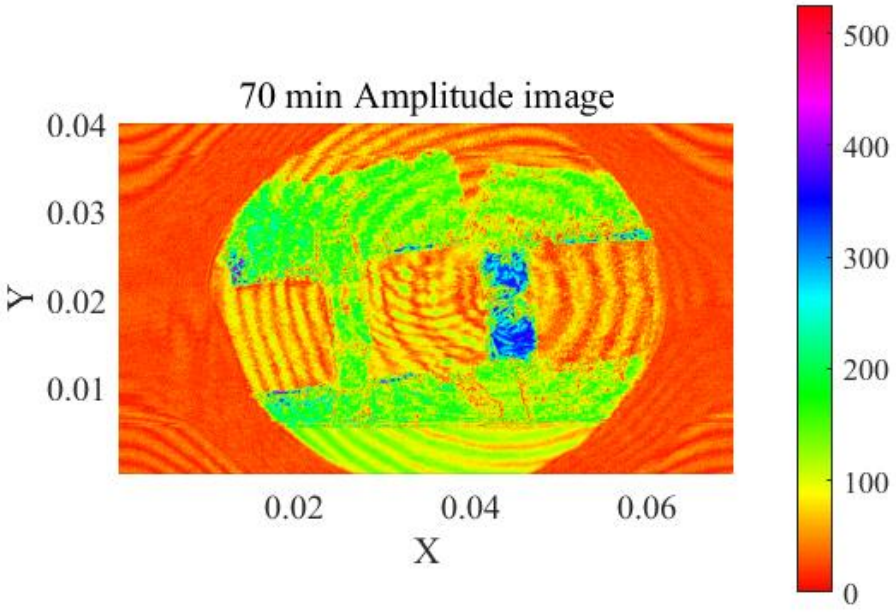

Figure 37. Amplitude image of 70 minutes

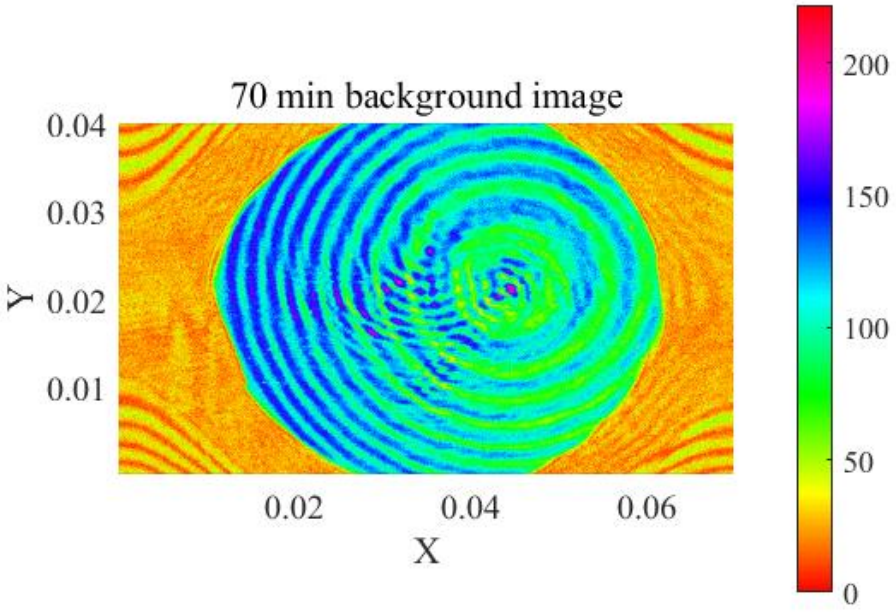

Figure 38. Background image of 70 minutes

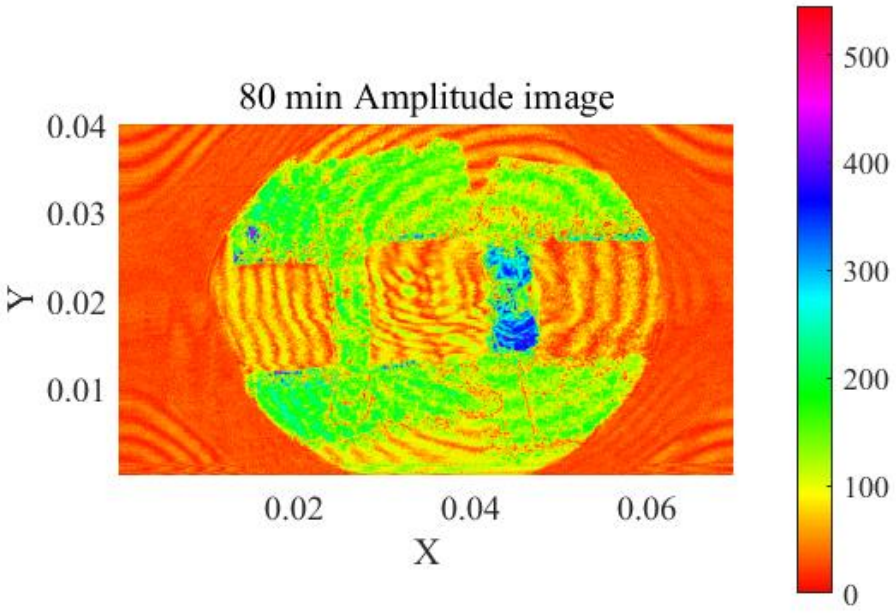

Figure 39. Amplitude image of 80 minutes

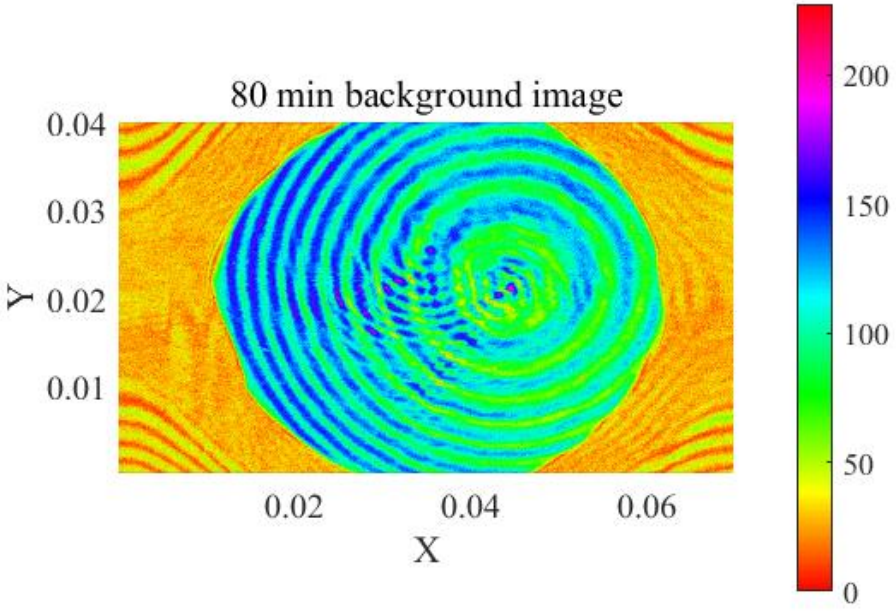

Figure 40. Background image of 80 minutes

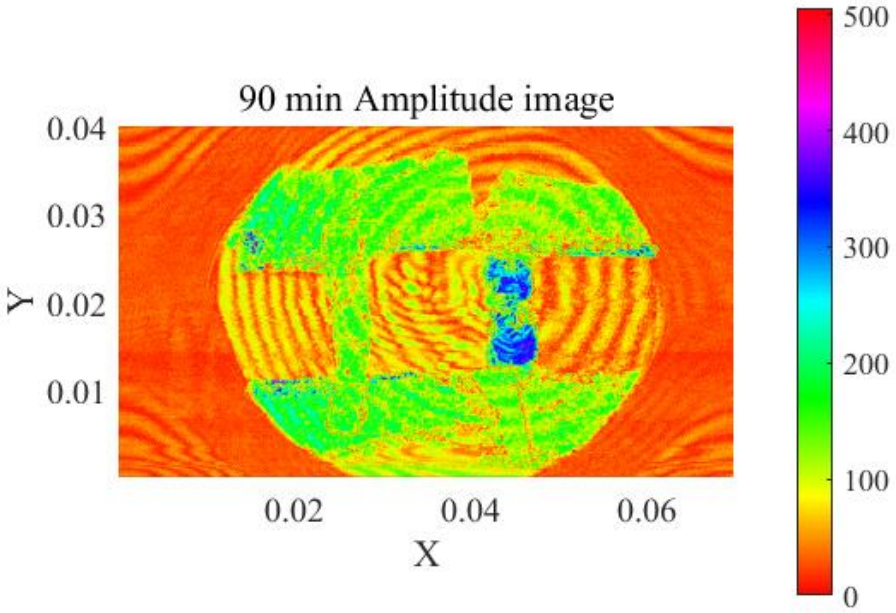

Figure 41. Amplitude image of 90 minutes

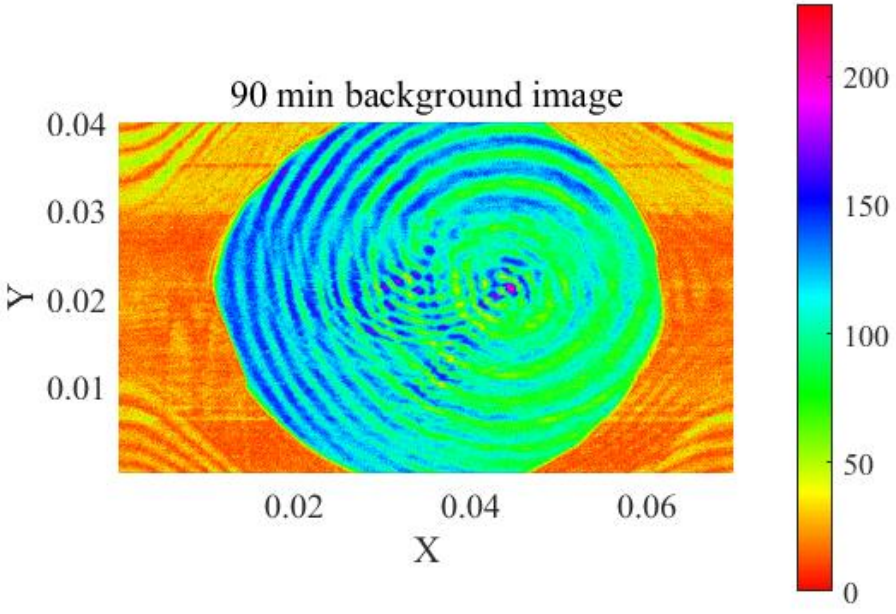

Figure 42. Background image of 90 minutes

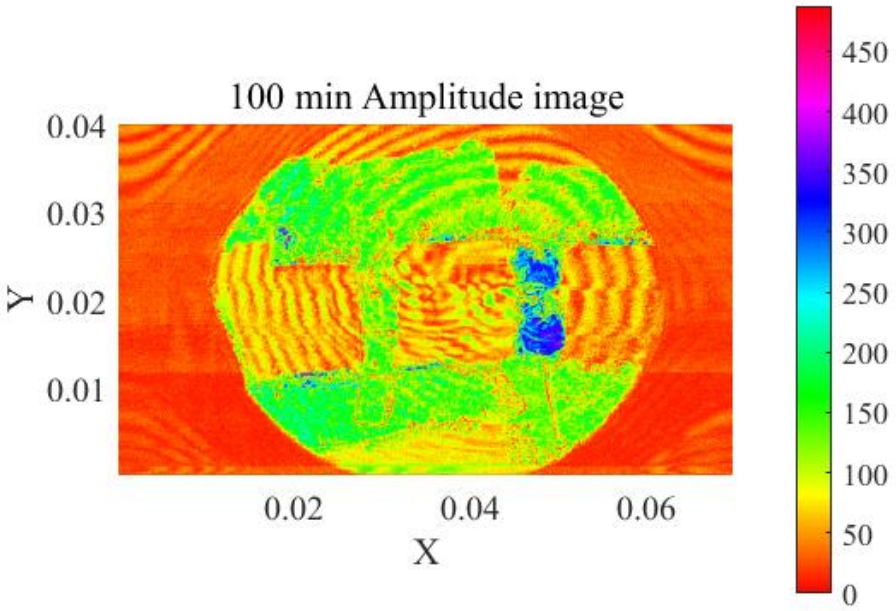

Figure 43. Amplitude image of 100 minutes Figure

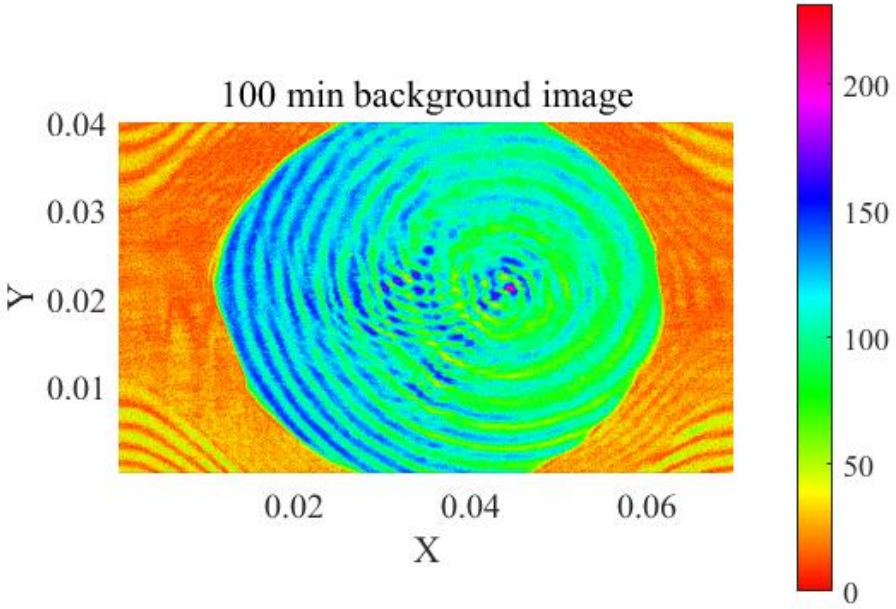

Figure 44. Background image of 100 minutes

To eliminate the effect of Newton's rings, it is necessary to optimize and adjust the data. Taking a 10-minute scan image as an example, we first read the data of the arm scan at the 10-minute mark and the corresponding blank scan data preceding it. Then, we divided the arm scan data by the blank data. The following are ten images of the processed data.

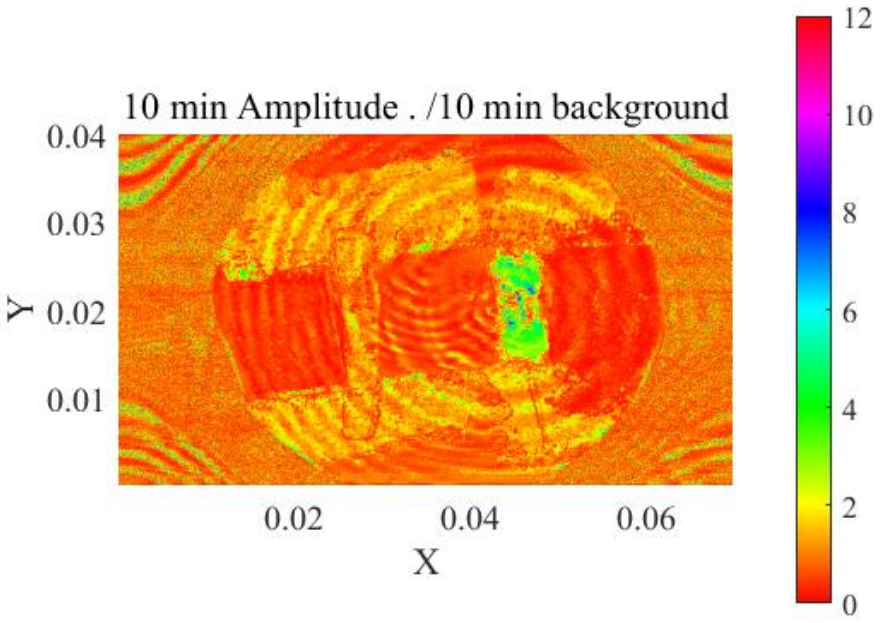

Figure 45. 10 min processed division data image.

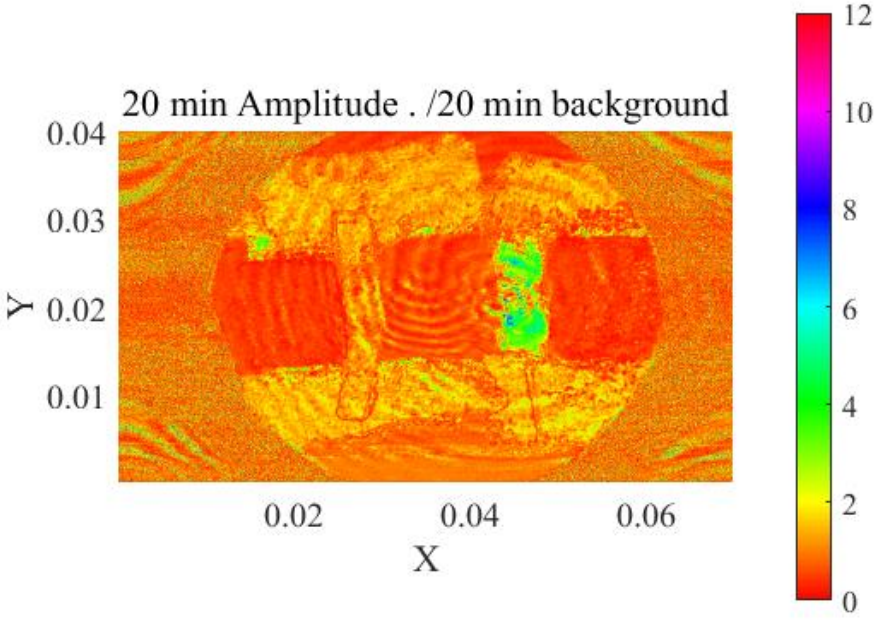

Figure 46. 20 min processed division data image.

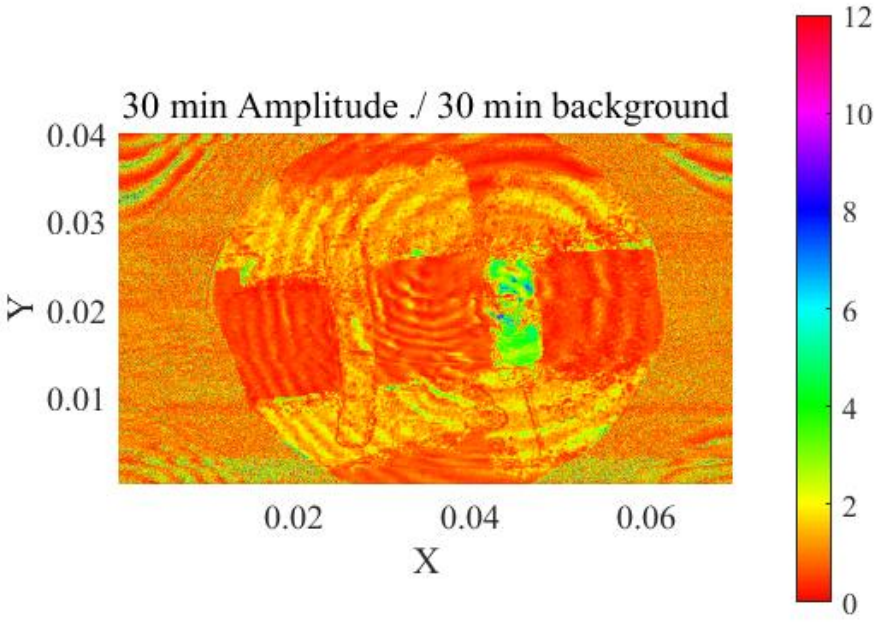

Figure 47. 30 min processed division data image.

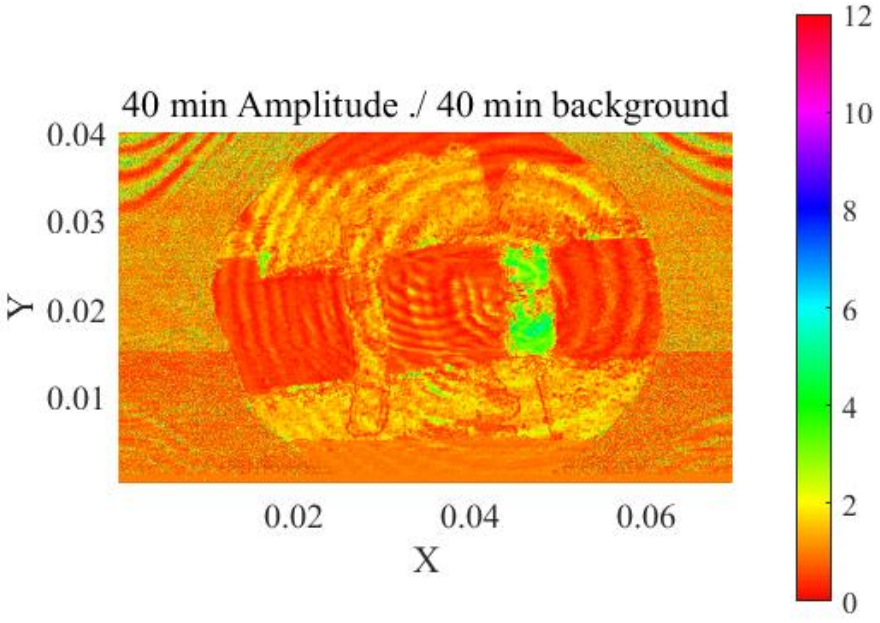

Figure 48. 40 min processed division data image.

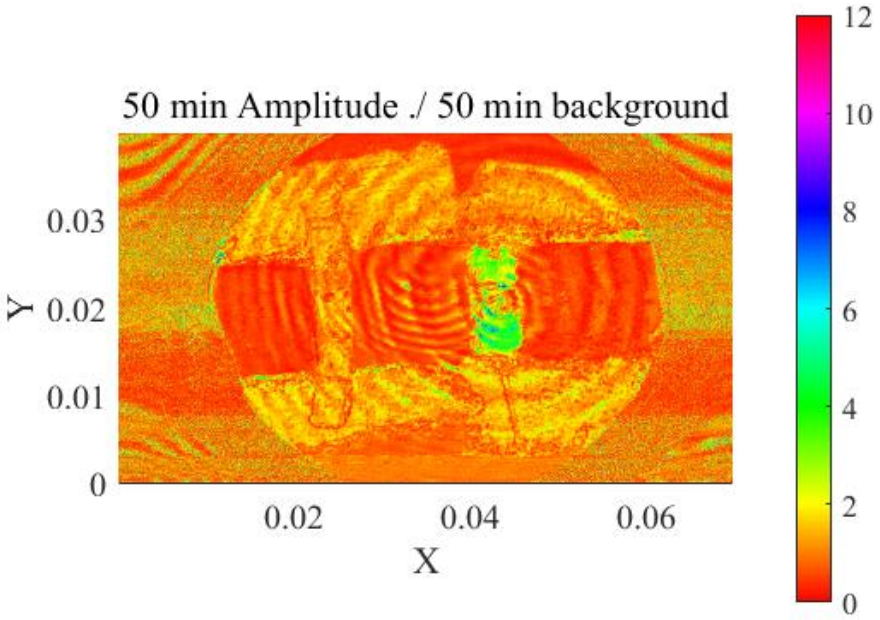

Figure 49. 50 min processed division data image.

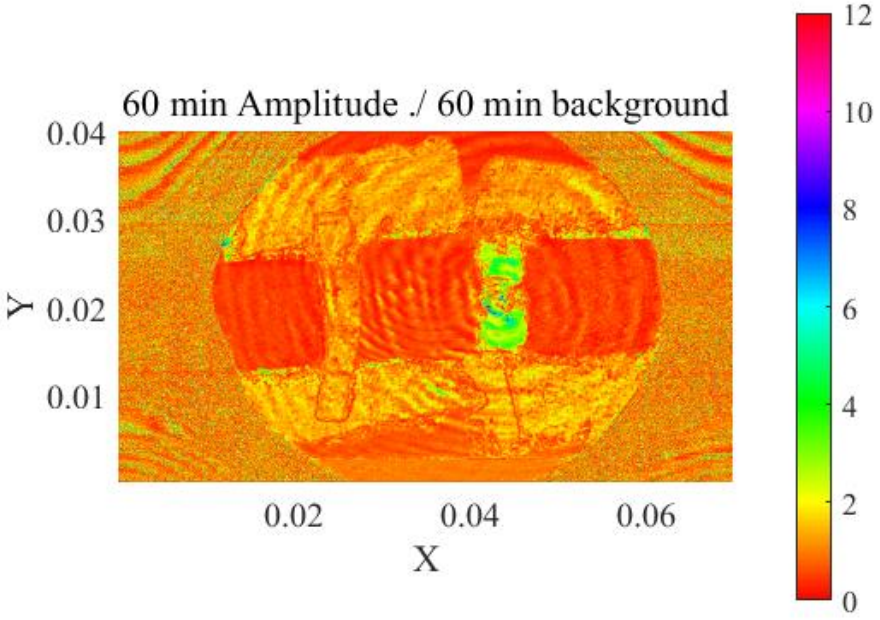

Figure 50. 60 min processed division data image.

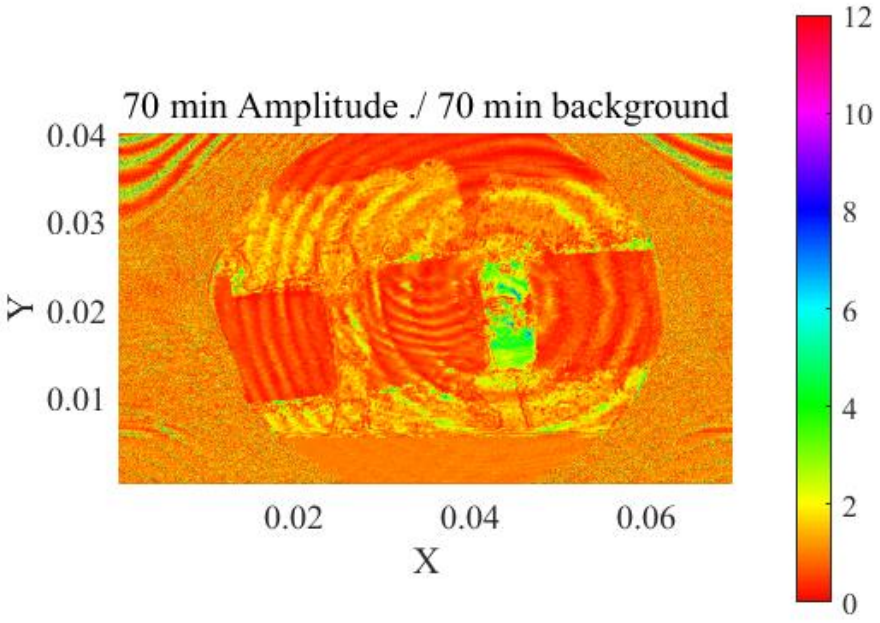

Figure 51. 70 min processed division data image.

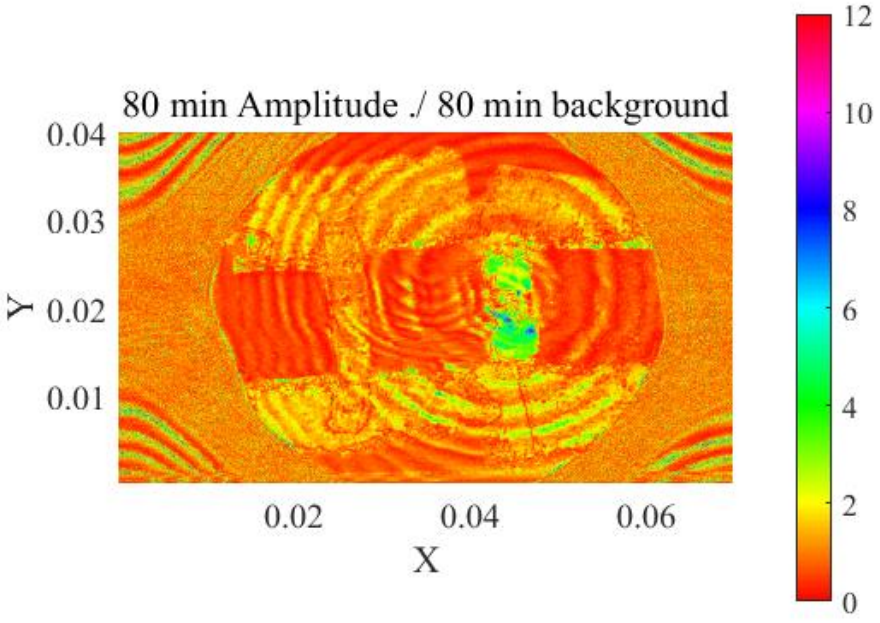

Figure 52. 80 min processed division data image.

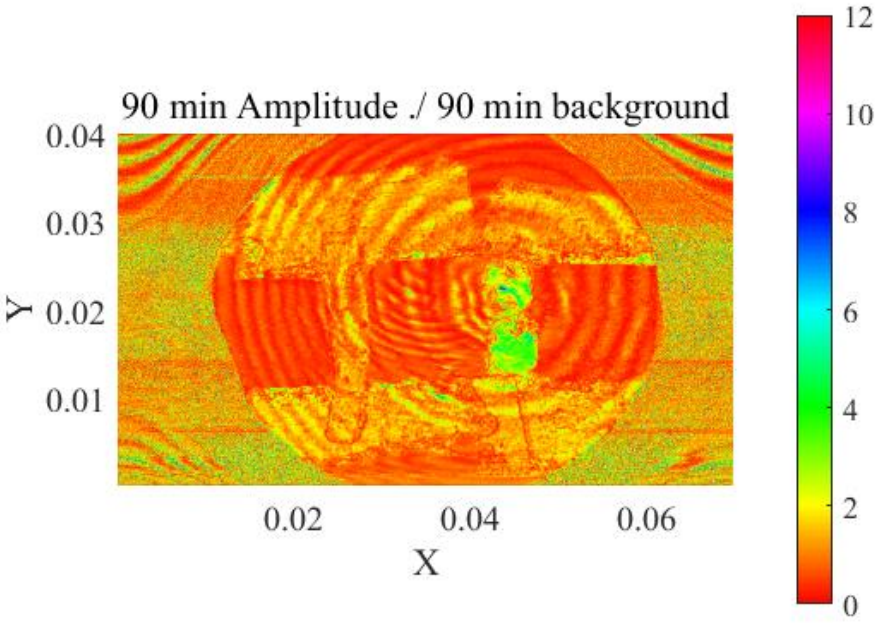

Figure 53. 90 min processed division data image.

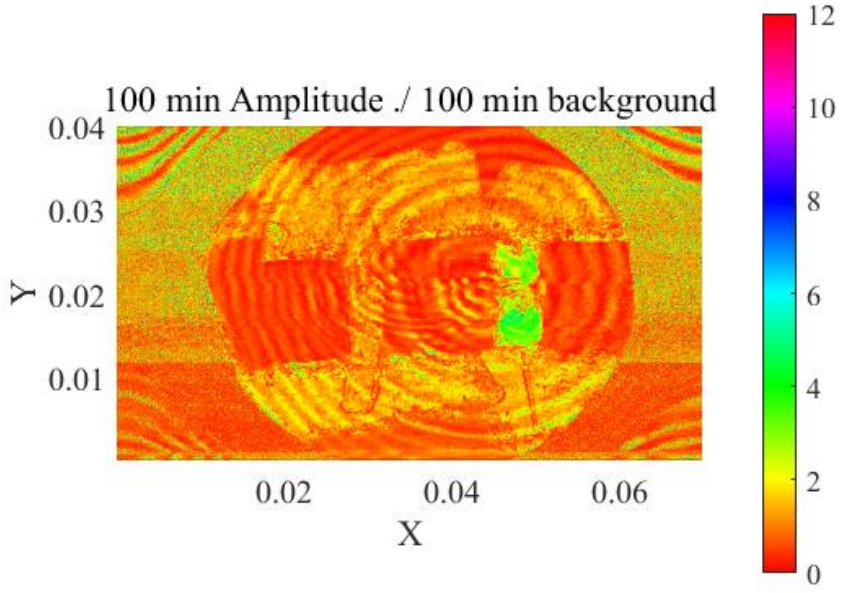

Figure 54. 100 min processed division data image.

ii. Processing data

In each processed image, a 70×130 pixel rectangular area was selected from three distinct regions. Following manual adjustment of the matrix coordinates, the mean value of each matrix in these regions was calculated using the averaging function. After processing all ten data sets, a graph (Figure 55) was generated to illustrate the relationship between the average amplitude of the three regions and time over a period of 100 minutes.

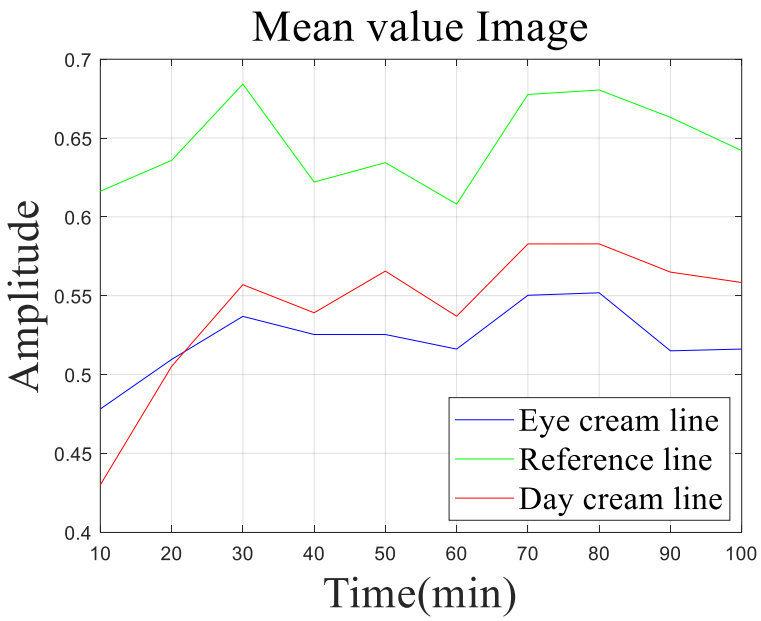

Figure 55. Mean value image of the final Thz experiment.

(red line) L'Oréal day cream. (blue line) L'Oréal eye cream. (green line) reference group.

Based on the data presented in Figure 55, it can be inferred that the changes in eye cream and day cream are influenced by environmental factors, as indicated by the reference group. To minimize the impact of the environment on the results, the data were normalized by subtracting the average values of the day cream and eye cream groups from the reference group average, respectively. The normalization data for the three areas across 10 measurements is shown in Figure 56.

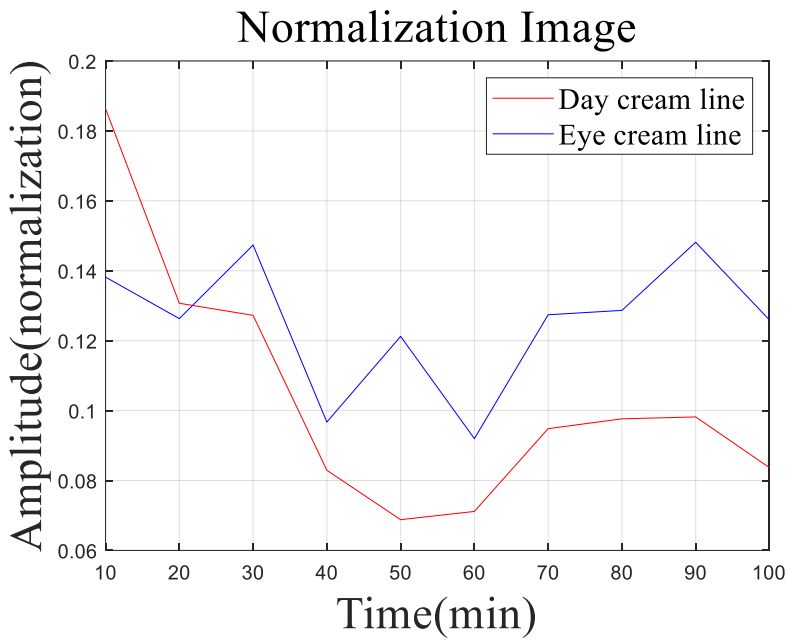

Figure 56. Normalization value image of the final Thz experiment.

(red line) L'Oréal day cream. (blue line) L'Oréal eye cream

iii. Analyzing data

Overall, both curves show a pattern of initial decrease followed by an increase in amplitude. Water exhibits a high absorption coefficient in the THZ frequency range [55], leading to significant absorption of THZ light upon encountering water. This also implies that higher moisture content will result in smaller signal amplitude. The data analysis revealed that during the initial 25 minutes, the moisturizing effect of the eye cream was more prominent than that of the day cream. Subsequently, the amplitude of the day cream gradually decreased in comparison to the eye cream. Within the first 50 minutes, both amplitudes decreased, indicating a gradual increase in skin hydration. It is evident that both day creams and eye creams contribute to moisturizing the skin to some extent. However, in the second half of the period, the amplitude of both gradually increased, indicating a gradual decrease in the water content of the skin. Figure 57 visualizes both day creams and eye creams in comparison and common trends using a timeline.

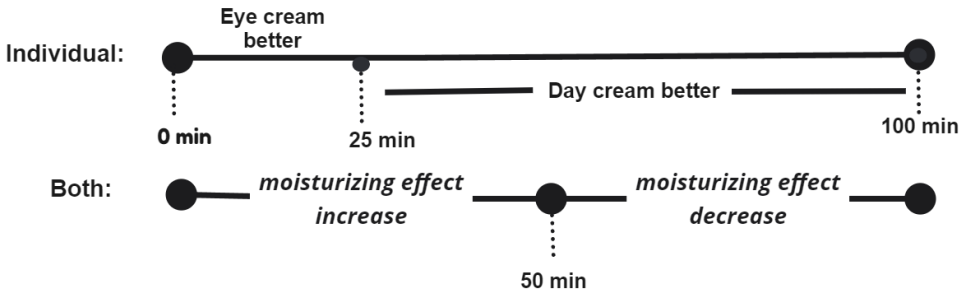

Figure 57. Trends of day cream and eye cream in the final Thz experiment

- **Corneometer CM825 experiment**

i. Visualization data

The software system of the CM825 automatically generates the mean and standard deviation of each measurement for all regions. We used MATLAB to analyse and process the data. Once the average hydration levels of the three areas over time are inputted into the matrix, the variance of each trial is depicted as an error bar. These error bars indicate the variability of each measurement and reflect the range over which the data points can extend. Figure 58 displays the results of the data handling.

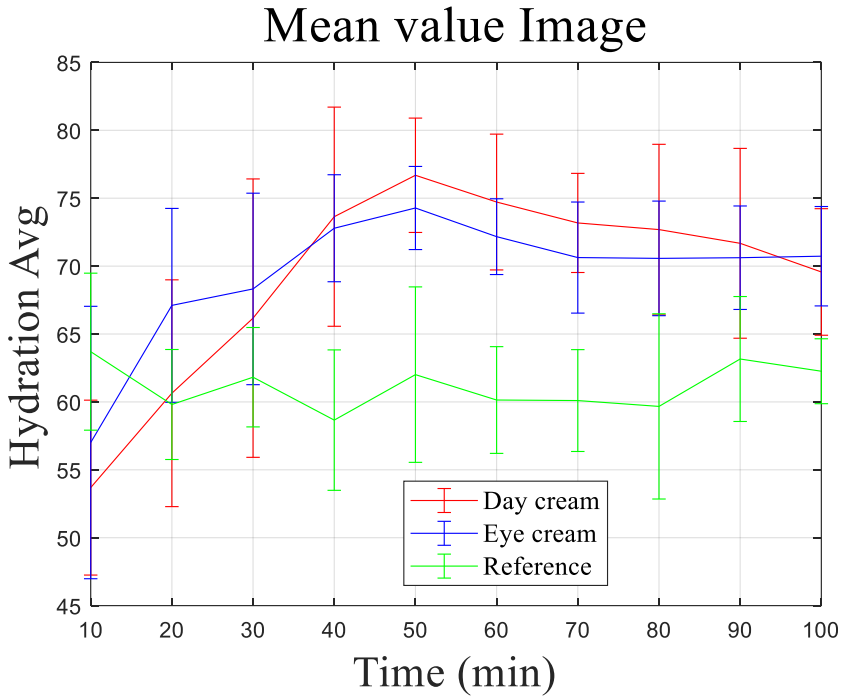

Figure 58. Mean value image of the final CM825 experiment.

(red line) L'Oréal day cream. (blue line) L'Oréal eye cream. (green line) reference group.

ii. Processing data

Similar to the QCL experiment, we normalized the mean values for the day cream and eye cream groups separately to minimize environmental effects. Figure 59 presents the normalized data across the 10 time periods.

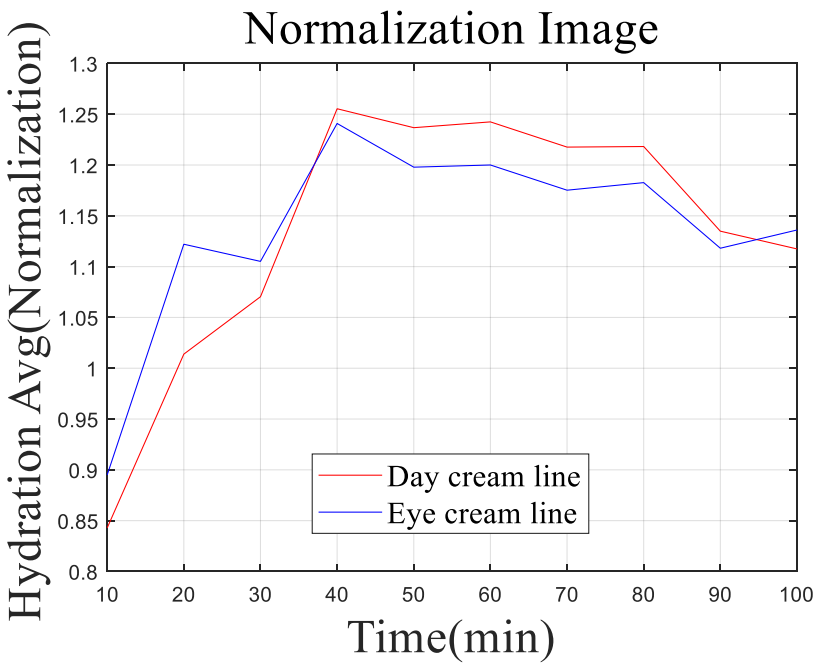

Figure 59. Normalization value image of the final CM825 experiment.

(red line) L'Oréal day cream. (blue line) L'Oréal eye cream

iii. Analyzing data

In terms of overall performance, both day and eye creams have shown an increasing trend in effectiveness for skin hydration, reaching a peak at around 40–50 minutes before gradually decreasing. The fluctuations of the reference series did not change significantly, and its average water content values remained in the range of 60-65. Day creams and eye creams generally maintain higher levels of hydration compared to the reference collection, which indicates their potential efficacy. During the first 40 minutes of the experiment, the moisturising effect of eye cream was slightly greater than that of day cream, but towards the end of the 40 minutes, the hydration levels of the two creams were approaching the same amount. Then, the value of the day cream exceeded that of the eye cream. After 50 minutes, the moisturizing effect of the day cream gradually decreased from its peak of 76.69, while that of the eye cream declined from 74.28. Both products showed a weakening in their hydrating effectiveness throughout this duration of time.

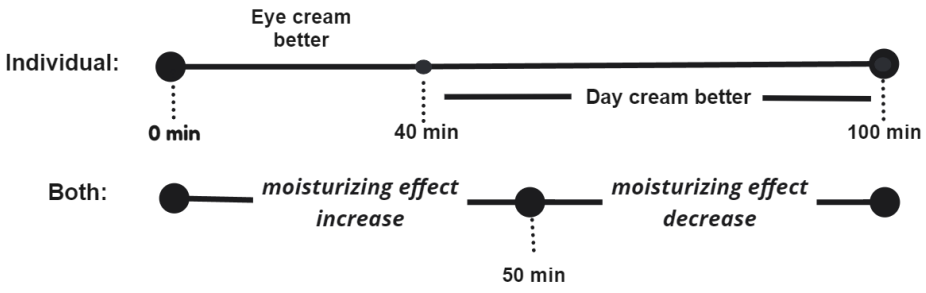

Figure 60. Trends of day cream and eye cream in the CM825 experiment

6.4.4 Discussion

To observe the trends more intuitively in skin water content over time as measured by the two experiments, we attempted to present their results in a single graph(). Since the results and interpretations of the QCL experiment and the CM835 experiment differ, it was necessary to normalize the curve data. By normalizing all curves using their respective maximum values, the maximum data value was set to 1. However, since the QCL data units are amplitude, which is inversely related to skin hydration, we multiplied the QCL data by -1 to accurately reflect its trend.

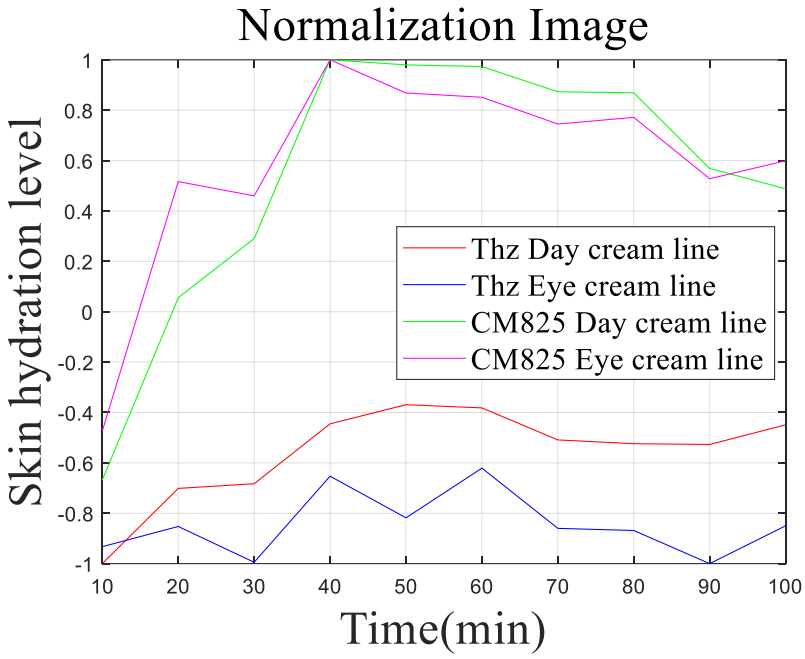

Figure 61. Two experiments normalization value image.

(green line) CM825 L'Oréal day cream. (pink line) CM825 L'Oréal eye cream.
(red line) Thz L'Oréal day cream. (blue line) Thz L'Oréal eye cream.

The curves of the results of both experiments demonstrate that the moisture content of the skin shows an increasing and then decreasing trend.

Firstly, the decline in water content values in the later stages may be due to the evaporation of some moisturizing components over time, thereby reducing the moisturizing effect of both products on the skin's surface. Secondly, the CM825 measures at a depth of 10-20 μm[56], while the QCL also detects in the range of 10 to 30 μm for the skin [57]. The thickness of the stratum corneum of the human forearm usually stays between 10 and 20 μm [58]. Throughout the 100-minute-long experiment, the chemicals in both types of skin care products have likely entered the skin tissue deeper than the stratum corneum. This led to the results detected by CM825 and QC showing a decreasing trend in water content at a later stage.

In addition, the moisturizing effect of the eye cream was also reflected in the experiment by showing up faster than the day cream. The reason for this outcome is most likely due to their different ingredients. According to the product information on L'Oreal's website, both the day cream and the eye cream include skin care basics such as water and glycerin. On top of that, the day cream includes ingredients like Myristyl Myristate and Butyrospermum Parkii Butter [59]. While the eye cream has moisturizing ingredients like Shorea Robusta Butter [60]. While day creams focus on the entire face, eye creams focus more on the skin around the eyes. As a result, there may be a discrepancy in the rate at which their moisturizing ingredients enter the skin barrier.

Chapter 7. General Discussion and Conclusions

7.1 Conclusions

Using terahertz imaging based on laser feedback interferometry, we monitored the effects of different creams on skin moisture in real-time. The experimental results showed that both creams led to a trend of first increase and then decrease in skin moisture content, and the later decline in both results may be caused by the evaporation of some moisturizing ingredients and the deep penetration of chemicals. The moisturizing effect of both day and eye creams was demonstrated in the experiment, and the difference in ingredients between the two may have resulted in the hydrating effect of the eye cream appearing faster than that of the day cream.

Overall, terahertz imaging technology demonstrates its great potential for skin care product evaluation. Its high resolution and rapid data acquisition capabilities provide detailed information on skin moisture changes that can assist in the scientific evaluation and development of skincare products. This technology could not only open up a new direction for the skincare field but also provide consumers with more reliable verification of product efficacy.

7.2 Future Work

Future research could further explore the application of terahertz imaging in different types of skin care products and how to optimize experimental factors to obtain more accurate measurements. For example, as with the experiment set up in [46], use a pressure sensor to ensure that the force on the arm is equalized. In addition to this, choose to experiment when the system is stable without its Newtonian ring background, and minimize the influence of environmental signals on the experiment. At the same time, more measurements can be combined and compared to ensure the reliability and accuracy of the data. This will provide the skincare industry with a more comprehensive product evaluation tool, which will help to promote the progress and innovation of skincare technology.

Chapter 8. References

[1] S. Verdier-Sévrain and F. Bonté, 'Skin hydration: a review on its molecular mechanisms', *J. Cosmet. Dermatol.*, vol. 6, no. 2, pp. 75–82, 2007, doi: 10.1111/j.1473-2165.2007.00300.x.

[2] I. H. Blank, 'Factors Which Influence the Water Content of the Stratum Corneum', *J. Invest. Dermatol.*, vol. 18, no. 6, pp. 433–440, Jun. 1952, doi: 10.1038/jid.1952.52.

[3] I. H. Blank and E. B. Shappirio, 'The Water Content of the Stratum Corneum', *J. Invest. Dermatol.*, vol. 25, no. 6, pp. 391–401, Dec. 1955, doi: 10.1038/jid.1955.145.

[4] D. I. Ramos-Soto, A. K. Singh, E. Saucedo-Casas, E. Castro-Camus, and M. Alfaro-Gomez, 'Visualization of moisturizer effects in stratum corneum in vitro using THz spectroscopic imaging', *Appl. Opt.*, vol. 58, no. 24, pp. 6581–6585, Aug. 2019, doi: 10.1364/AO.58.006581.

[5] H. Lindley-Hatcher, A. I. Hernandez-Serrano, J. Wang, J. Cebrian, J. Hardwicke, and E. Pickwell-MacPherson, 'Evaluation of in vivo THz sensing for assessing human skin hydration', *J. Phys. Photonics*, vol. 3, no. 1, p. 014001, Jan. 2021, doi: 10.1088/2515-7647/abcb71.

[6] P. u. Jepsen, D. g. Cooke, and M. Koch, 'Terahertz spectroscopy and imaging – Modern techniques and applications', *Laser Photonics Rev.*, vol. 5, no. 1, pp. 124–166, 2011, doi: 10.1002/lpor.201000011.

[7] P. Dean *et al.*, 'Terahertz imaging using quantum cascade lasers—a review of systems and applications', *J. Phys. Appl. Phys.*, vol. 47, no. 37, p. 374008, Sep. 2014, doi: 10.1088/0022-3727/47/37/374008.

[8] A. D. Rakić *et al.*, 'Swept-frequency feedback interferometry using terahertz frequency QCLs: a method for imaging and materials analysis', *Opt. Express*, vol. 21, no. 19, pp. 22194–22205, Sep. 2013, doi: 10.1364/OE.21.022194.

[9] E. Berardesca and European Group for Efficacy Measurements on Cosmetics and Other Topical Products (EEMCO), 'EEMCO guidance for the assessment of stratum corneum hydration: electrical methods', *Skin Res. Technol.*, vol. 3, no. 2, pp. 126–132, 1997, doi: 10.1111/j.1600-0846.1997.tb00174.x.

[10] M.-M. CONSTANTIN, E. POENARU, C. POENARU, and T. CONSTANTIN, 'Skin Hydration Assessment through Modern Non-Invasive Bioengineering Technologies', *Mædica*, vol. 9, no. 1, pp. 33–38, Mar. 2014.

[11] U. Heinrich *et al.*, ‘Multicentre comparison of skin hydration in terms of physical-, physiological- and product-dependent parameters by the capacitive method (Corneometer CM 825)’, *Int. J. Cosmet. Sci.*, vol. 25, no. 1–2, pp. 45–53, 2003, doi: 10.1046/j.1467-2494.2003.00172.x.

[12] J. m. Crowther, ‘Understanding effects of topical ingredients on electrical measurement of skin hydration’, *Int. J. Cosmet. Sci.*, vol. 38, no. 6, pp. 589–598, 2016, doi: 10.1111/ics.12324.

[13] E. Berardesca, M. Loden, J. Serup, P. Masson, and L. M. Rodrigues, ‘The revised EEMCO guidance for the in vivo measurement of water in the skin’, *Skin Res. Technol.*, vol. 24, no. 3, pp. 351–358, 2018, doi: 10.1111/srt.12599.

[14] P. Clarys, R. Clijsen, and A. O. Barel, ‘Influence of probe application pressure on in vitro and in vivo capacitance (Corneometer CM 825®) and conductance (Skicon 200 EX®) measurements’, *Skin Res. Technol.*, vol. 17, no. 4, pp. 445–450, 2011, doi: 10.1111/j.1600-0846.2011.00516.x.

[15] K. O’goshi and J. Serup, ‘Skin conductance; validation of Skicon-200EX® compared to the original model, Skicon-100®’, *Skin Res. Technol.*, vol. 13, no. 1, pp. 13–18, 2007, doi: 10.1111/j.1600-0846.2006.00200.x.

[16] P. Clarys, R. Clijsen, J. Taeymans, and A. O. Barel, ‘Hydration measurements of the stratum corneum: comparison between the capacitance method (digital version of the Corneometer CM 825®) and the impedance method (Skicon-200EX®)’, *Skin Res. Technol.*, vol. 18, no. 3, pp. 316–323, 2012, doi: 10.1111/j.1600-0846.2011.00573.x.

[17] D. c. Salter, R. j. Hodgson, L. d. Hall, T. a. Carpenter, and S. Ablett, ‘Moisturization processes in living human skin studied by magnetic resonance imaging microscopy’, *Int. J. Cosmet. Sci.*, vol. 15, no. 5, pp. 219–226, 1993, doi: 10.1111/j.1467-2494.1993.tb00076.x.

[18] S. Richard *et al.*, ‘Characterization of the Skin *In Vivo* by High Resolution Magnetic Resonance Imaging: Water Behavior and Age-Related Effects’, *J. Invest. Dermatol.*, vol. 100, no. 5, pp. 705–709, May 1993, doi: 10.1111/1523-1747.ep12472356.

[19] R.-J. M. van Geuns *et al.*, ‘Basic principles of magnetic resonance imaging’, *Prog. Cardiovasc. Dis.*, vol. 42, no. 2, pp. 149–156, Sep. 1999, doi: 10.1016/S0033-0620(99)70014-9.

[20] F. Mirrashed and J. C. Sharp, ‘In vivo morphological characterisation of the skin by MRI micro-imaging methods’, *Skin Res. Technol.*, vol. 10, no. 3, pp. 149–160, 2004, doi: 10.1111/j.1600-0846.2004.00071.x.

[21] A. Sakata, K. Abe, K. Mizukoshi, T. Gomi, and I. Okuda, ‘Relationship between the retinacula cutis and sagging facial skin’, *Skin Res. Technol.*, vol. 24, no. 1, pp. 93–98, 2018, doi: 10.1111/srt.12395.

[22] B. Querleux, ‘Multimodal Magnetic Resonance Imaging of the Human Skin’, in *Non Invasive Diagnostic Techniques in Clinical Dermatology*, E. Berardesca, H. I. Maibach, and K.-P. Wilhelm, Eds., Berlin, Heidelberg: Springer, 2014, pp. 169–176. doi: 10.1007/978-3-642-32109-2_15.

[23] D. Singh, A. Monga, H. L. de Moura, X. Zhang, M. V. W. Zibetti, and R. R. Regatte, ‘Emerging Trends in Fast MRI Using Deep-Learning Reconstruction on Undersampled k-Space Data: A Systematic Review’, *Bioengineering*, vol. 10, no. 9, Art. no. 9, Sep. 2023, doi: 10.3390/bioengineering10091012.

[24] M. I. Anik, M. K. Hossain, I. Hossain, I. Ahmed, and R. M. Doha, ‘18 - Biomedical applications of magnetic nanoparticles’, in *Magnetic Nanoparticle-Based Hybrid Materials*, A. Ehrmann, T. A. Nguyen, M. Ahmadi, A. Farmani, and P. Nguyen-Tri, Eds., in Woodhead Publishing Series in Electronic and Optical Materials. , Woodhead Publishing, 2021, pp. 463–497. doi: 10.1016/B978-0-12-823688-8.00002-8.

[25] X. Wortsman, ‘Practical applications of ultrasound in dermatology’, *Clin. Dermatol.*, vol. 39, no. 4, pp. 605–623, Jul. 2021, doi: 10.1016/j.clindermatol.2021.03.007.

[26] N. Almuhanna, X. Wortsman, I. Wohlmuth-Wieser, M. Kinoshita-Ise, and R. Alhusayen, ‘Overview of Ultrasound Imaging Applications in Dermatology’, *J. Cutan. Med. Surg.*, vol. 25, no. 5, pp. 521–529, Sep. 2021, doi: 10.1177/1203475421999326.

[27] R. Kleinerman, T. B. Whang, R. L. Bard, and E. S. Marmur, ‘Ultrasound in dermatology: Principles and applications’, *J. Am. Acad. Dermatol.*, vol. 67, no. 3, pp. 478–487, Sep. 2012, doi: 10.1016/j.jaad.2011.12.016.

[28] C. Eisenbeiss, J. Welzel, W. Eichler, and K. Klotz, ‘Influence of body water distribution on skin thickness: measurements using high-frequency ultrasound’, *Br. J. Dermatol.*, vol. 144, no. 5, pp. 947–951, May 2001, doi: 10.1046/j.1365-2133.2001.04180.x.

[29] R. K. Mlosek *et al.*, ‘The use of high frequency ultrasound imaging in skin moisturization measurement’, *Skin Res. Technol.*, vol. 19, no. 2, pp. 169–175, 2013, doi: 10.1111/srt.12029.

[30] O. A. Smolyanskaya *et al.*, ‘Terahertz biophotonics as a tool for studies of dielectric and spectral properties of biological tissues and liquids’, *Prog. Quantum Electron.*, vol. 62, pp. 1–77, Nov. 2018, doi: 10.1016/j.pquantelec.2018.10.001.

[31] J. Neu and C. A. Schmuttenmaer, ‘Tutorial: An introduction to terahertz time domain spectroscopy (THz-TDS)’, *J. Appl. Phys.*, vol. 124, no. 23, p. 231101, Dec. 2018, doi: 10.1063/1.5047659.

[32] Z. D. Taylor *et al.*, ‘THz Medical Imaging: in vivo Hydration Sensing’, *IEEE Trans. Terahertz Sci. Technol.*, vol. 1, no. 1, pp. 201–219, Sep. 2011, doi: 10.1109/TTHZ.2011.2159551.

[33] G. G. Hernandez-Cardoso *et al.*, ‘Terahertz imaging for early screening of diabetic foot syndrome: A proof of concept’, *Sci. Rep.*, vol. 7, no. 1, Art. no. 1, Feb. 2017, doi: 10.1038/srep42124.

[34] S. Fan, B. S. Y. Ung, E. P. J. Parrott, V. P. Wallace, and E. Pickwell-MacPherson, ‘In vivo terahertz reflection imaging of human scars during and after the healing process’, *J. Biophotonics*, vol. 10, no. 9, pp. 1143–1151, 2017, doi: 10.1002/jbio.201600171.

[35] N. Jukam *et al.*, ‘Terahertz amplifier based on gain switching in a quantum cascade laser’, *Nat. Photonics*, vol. 3, no. 12, pp. 715–719, Dec. 2009, doi: 10.1038/nphoton.2009.213.

[36] K. Singh *et al.*, ‘Comparison of Physical and System Factors Impacting Hydration Sensing in Leaves Using Terahertz Time-Domain and Quantum Cascade Laser Feedback Interferometry Imaging’, *Sensors*, vol. 23, no. 5, Art. no. 5, Jan. 2023, doi: 10.3390/s23052721.

[37] L. Esaki and R. Tsu, ‘Superlattice and Negative Differential Conductivity in Semiconductors’, *IBM J. Res. Dev.*, vol. 14, no. 1, pp. 61–65, Jan. 1970, doi: 10.1147/rd.141.0061.

[38] J. Faist, F. Capasso, D. L. Sivco, C. Sirtori, A. L. Hutchinson, and A. Y. Cho, ‘Quantum cascade laser’, *Science*, vol. 264, no. 5158, pp. 553–556, Apr. 1994, doi: 10.1126/science.264.5158.553.

[39] W. L. Chan, J. Deibel, and D. M. Mittleman, ‘Imaging with terahertz radiation’, *Rep. Prog. Phys.*, vol. 70, no. 8, p. 1325, Jul. 2007, doi: 10.1088/0034-4885/70/8/R02.

[40] S. Kumar, ‘Recent Progress in Terahertz Quantum Cascade Lasers’, *IEEE J. Sel. Top. Quantum Electron.*, vol. 17, no. 1, pp. 38–47, Jan. 2011, doi: 10.1109/JSTQE.2010.2049735.

[41] D. L. Woolard, R. Brown, M. Pepper, and M. Kemp, ‘Terahertz Frequency Sensing and Imaging: A Time of Reckoning Future Applications?’, *Proc. IEEE*, vol. 93, no. 10, pp. 1722–1743, Oct. 2005, doi: 10.1109/JPROC.2005.853539.

[42] L. Li *et al.*, ‘Terahertz quantum cascade lasers with >1 W output powers’, *Electron. Lett.*, vol. 50, no. 4, pp. 309–311, 2014, doi: 10.1049/el.2013.4035.

[43] T. S. SOLUTIONS DRS DAYLIGHT, ‘Quantum Cascade Lasers Shift from an Emerging to an Enabling Technology’. Accessed: May 31, 2024. [Online]. Available: https://www.photonics.com/Articles/Quantum_Cascade_Lasers_Shift_from_an_Emerging_to/a67658

[44] A. D. Rakić *et al.*, ‘Sensing and imaging using laser feedback interferometry with quantum cascade lasers’, *Appl. Phys. Rev.*, vol. 6, no. 2, p. 021320, Jun. 2019, doi: 10.1063/1.5094674.

[45] T. Taimre, M. Nikolić, K. Bertling, Y. L. Lim, T. Bosch, and A. D. Rakić, ‘Laser feedback interferometry: a tutorial on the self-mixing effect for coherent sensing’, *Adv. Opt. Photonics*, vol. 7, no. 3, pp. 570–631, Sep. 2015, doi: 10.1364/AOP.7.000570.

[46] H. R. Zelsmann, ‘Temperature dependence of the optical constants for liquid H2O and D2O in the far IR region’, *J. Mol. Struct.*, vol. 350, no. 2, pp. 95–114, May 1995, doi: 10.1016/0022-2860(94)08471-S.

[47] Y. L. Lim *et al.*, ‘Coherent imaging using laser feedback interferometry with pulsed-mode terahertz quantum cascade lasers’, *Opt. Express*, vol. 27, no. 7, pp. 10221–10233, Apr. 2019, doi: 10.1364/OE.27.010221.

[48] R. Kohler, A. Tredicucci, F. Beltram, H. E. Beere, and et al, ‘Terahertz semiconductor-heterostructure laser’, *Nature*, vol. 417, no. 6885, pp. 156–9, May 2002, doi: 10.1038/417156a.

[49] Y. L. Lim *et al.*, ‘High-contrast coherent terahertz imaging of porcine tissue via swept-frequency feedback interferometry’, *Biomed. Opt. Express*, vol. 5, no. 11, pp. 3981–3989, Nov. 2014, doi: 10.1364/BOE.5.003981.

[50] J. Darmo *et al.*, ‘Imaging with a Terahertz quantum cascade laser’, *Opt. Express*, vol. 12, no. 9, pp. 1879–1884, May 2004, doi: 10.1364/OPEX.12.001879.

[51] S. M. Kim *et al.*, ‘Biomedical terahertz imaging with a quantum cascade laser’, *Appl. Phys. Lett.*, vol. 88, no. 15, p. 153903, Apr. 2006, doi: 10.1063/1.2194229.

[52] S. Fan, E. P. J. Parrott, B. S. Y. Ung, and E. Pickwell-MacPherson, ‘Calibration method to improve the accuracy of THz imaging and spectroscopy in reflection geometry’, *Photonics Res.*, vol. 4, no. 3, pp. A29–A35, Jun. 2016, doi: 10.1364/PRJ.4.000A29.

[53] Q. Sun, E. P. J. Parrott, Y. He, and E. Pickwell-MacPherson, ‘In vivo THz imaging of human skin: Accounting for occlusion effects’, *J. Biophotonics*, vol. 11, no. 2, p. e201700111, 2018, doi: 10.1002/jbio.201700111.

[54] J. Wang, R. I. Stantchev, Q. Sun, T.-W. Chiu, A. T. Ahuja, and E. P. MacPherson, ‘THz in vivo measurements: the effects of pressure on skin reflectivity’, *Biomed. Opt. Express*, vol. 9, no. 12, pp. 6467–6476, Dec. 2018, doi: 10.1364/BOE.9.006467.

[55] H. J. Liebe, G. A. Hufford, and T. Manabe, ‘A model for the complex permittivity of water at frequencies below 1 THz’, *Int. J. Infrared Millim. Waves*, vol. 12, no. 7, pp. 659–675, Jul. 1991, doi: 10.1007/BF01008897.

[56] ‘Corneometer® CM 825 - skin hydration measurement’. Accessed: May 31, 2024. [Online]. Available: https://www.enviroderm.co.uk/products/corneometer-cm-825

[57] X. Qi *et al.*, ‘Terahertz imaging of human skin pathologies using laser feedback interferometry with quantum cascade lasers’, *Biomed. Opt. Express*, vol. 14, no. 4, pp. 1393–1410, Mar. 2023, doi: 10.1364/BOE.480615.

[58] L. M. Russell, S. Wiedersberg, and M. B. Delgado-Charro, ‘The determination of stratum corneum thickness – an alternative approach’, *Eur. J. Pharm. Biopharm. Off. J. Arbeitsgemeinschaft Pharm. Verfahrenstechnik EV*, vol. 69, no. 3, pp. 861–870, Aug. 2008, doi: 10.1016/j.ejpb.2008.02.002.

[59] ‘Revitalift Classic skin-care Anti-Wrinkle + Extra-Firming Day Cream 50ml - For 40+’, L’Oréal Paris. Accessed: May 31, 2024. [Online]. Available: https://www.lorealparis.com.au/revitalift/classic/day-cream

[60] ‘Revitalift Classic skin-care Anti-Wrinkle + Extra-Firming Eye Cream 50ml - For 40’, L’Oréal Paris. Accessed: May 31, 2024. [Online]. Available: https://www.lorealparis.com.au/revitalift/classic/eye-cream

Chapter 9. Appendix. GitHub Repository

1. MATLAB Code of Thz-QCL & CM825 probe

Here is the DOI of the MATLAB Code of the Thz-QCL & CM825 probe experiment analysis.
If you prefer to check the code, ensure they are all in the same folder.
Some of the files are large, so downloading them will take a little while.

DOI: https://zenodo.org/records/11419814